Characterization of multilayer delaminations in composites using wavenumber analysis: numerical and experimental studies

Hanfei Mei and **Victor Giurgiutiu**

Abstract

Delamination is one of the most common and dangerous failure modes for composites because it takes place and grows in the absence of any visible surface damage. The successful implementation of delamination detection in aerospace composite structures is always challenging due to the general anisotropic behavior of composites and multilayer delamination scenarios. This article presents a numerical and experimental investigation to detect and characterize the multilayer delaminations in carbon fiber–reinforced polymer composite plates using guided waves and wavenumber analysis. Multiphysics three-dimensional finite element simulations of the composite plate with five different delamination scenarios are conducted to provide the out-of-plane wave motion for wavenumber analysis. The out-of-plane results from finite element simulations of one delamination and two delaminations are validated by the scanning laser Doppler vibrometer measurements. It is found that the wavenumber analysis can identify the plies between which the delamination occurs and evaluate the delamination severity by comparing the new wavenumbers due to the trapped waves in the delamination regions, which is potentially related to delamination severity. Both numerical and experimental results demonstrate a good capability for the detection and characterization of multilayer delaminations in composite structures.

Keywords

Structural health monitoring, multilayer delaminations, guided wave, wavenumber analysis, composites, finite element modeling, piezoelectric wafer active sensors

Introduction

Composite materials have been extensively used in aerospace structures due to their superior strength and stiffness, resistance to corrosion, design flexibility, and lightweight.[1] However, various damage modes exist (e.g. delamination, debonding, and impact damage) in composites and their detection and quantification are much more difficult than those in metallic materials.[2–6] Delamination is the most common and dangerous failure mode for composite materials, because it occurs and grows in the absence of any visible surface damage, making it difficult to detect by visual inspection. Due to the general anisotropic behavior[7] and complex damage scenarios, the successful implementation of delamination detection in composite structures is always challenging.

Many non-destructive testing (NDT) methods have been developed to detect and quantify the delamination in composite structures, such as eddy current,[8] X-rays, and ultrasound methods.[9–11] However, these NDT methods are often labor-intensive and depend heavily on the skill and experience of the operator. Structural health monitoring (SHM) technologies offer a promising alternative and involve collecting data from various sensors installed on structures to make reliable and cost-effective decisions.[12] In recent years, various SHM methods have been developed, such as electromechanical impedance (EMI),[13] acoustic emission (AE),[14] and guided wave–based methods.[15] Among them, guided waves have been studied extensively for delamination detection due to their ability to inspect a large area

Department of Mechanical Engineering, University of South Carolina, Columbia, SC, USA

Corresponding author:
Hanfei Mei, Department of Mechanical Engineering, University of South Carolina, 300 Main Street, Columbia, SC 29208, USA.
Email: hmei@email.sc.edu

while maintaining a sensitivity to various types of damage.[16–34]

In recent years, damage detection using the guided wavefield analysis has been widely investigated. In this method, a permanently installed piezoelectric wafer active sensor (PWAS) transducer was typically utilized to excite guided waves propagating in the composites, and guided wavefield was measured by a scanning laser Doppler vibrometer (SLDV). The delamination can be unveiled through wavefield analysis, such as the wavefield amplitude profile,[19] frequency–wavenumber analysis,[20] and local wavenumber analysis.[21–25] Staszewski et al.[19] used the wavefield amplitude profiles to locate the delamination and estimate its severity in composite laminates. Tian et al.[20] applied the frequency–wavenumber analysis to detect and quantify a single-layer delamination, showing that wavenumber methods can not only determine the delaminated region but also identify the plies between which the delamination occurs. Rogge and Leckey[21] presented a local wavenumber domain analysis to process the wavefield, and they demonstrated that it could be used to quantify the delamination depth and size.

Moreover, various wavenumber imaging methods were applied for improved visualization of delamination in composites, such as frequency–wavenumber filtering,[26–28] standing wave filtering,[29] zero-lag cross-correlation (ZLCC) imaging,[30,31] time-reversal imaging,[32] spatial wavenumber imaging,[33] and wavenumber adaptive image filtering.[34] Sohn et al.[29] designed a standing wave filter to remove propagating waves from the wavefield and obtain standing waves in the delamination region for damage visualization. Girolamo et al.[31] applied the ZLCC imaging condition for visualizing impact damage in a honeycomb composite panel. Tian et al.[33] improved the damage visualization algorithm using the filtering reconstruction imaging and spatial wavenumber imaging. Kudela et al.[34] utilized the wavenumber adaptive image filtering to detect and visualize the impact-induced delaminations under different impact energies.

Computational wave simulation has proven to be an effective tool for clarifying complex ultrasonic wave phenomena. Previous investigators have reported the use of numerical simulations to study guided wave propagation and interaction with delaminations.[35–44] Guo and Cawley[35] used a two-dimensional (2D) finite element method (FEM) with plane strain assumption to study the reflection of the S0 mode from a delamination in unidirectional and cross-ply laminates. Ramadas et al.[36,37] investigated the A0 mode interaction with the symmetric and asymmetric delaminations using a 2D model. They showed that the mode-converted S0 mode was confined only to the sublaminates within the delamination region and converts back to the A0 mode

when exiting the delamination that is symmetrically located across the thickness, while the propagation of S0 mode in the main laminate was observed when A0 mode interacts with the delamination that is located asymmetrically across the thickness. Munian et al.[38] used a 2D time-domain spectral finite element (TSFE) method to investigate the interaction between guided waves and the delamination. However, all the aforementioned studies are limited to 2D situations which consider the delamination to be across the full width of the composite laminates. To solve this problem, three-dimensional (3D) finite element (FE) simulations were conducted to investigate guided wave interactions with the delaminations in a more realistic way and the scattering characteristics in different directions.[39–41] More recently, Leckey et al.[39] presented the benchmark studies of four different simulation tools, three commercial packages COMSOL, ABAQUS, and ANSYS, and a custom code, elastodynamic finite integration technique (EFIT), for 3D modeling of guided wave interaction with single delamination in composites. Ng and Veidt[40] investigated the scattering directivity pattern of a single delamination in a quasi-isotropic laminate using an experimentally validated 3D FE model. They showed that the behavior of the backward scattering amplitude is generally more complicated than that of the forward scattering amplitude and is generally smaller in magnitude particularly for larger delamination.

However, prior studies in the literature have focused on single delamination scenarios (i.e. a single delamination through the composite thickness). Leckey and Seebo[42] conducted a preliminary simulation to investigate differences in trapped energy for multilayer delaminations, and their studies showed that the trapped energy increases at the composite surface when additional delaminations exist through the composite thickness. In addition, 3D modeling of guided wave propagation and interaction with the actual impact damage was investigated in Leckey et al.[43] and Zhang et al.[44] These studies have facilitated our understanding of guided wave–based delamination detection using wavefield analysis. However, the numerical and experimental characterization of guided wave interactions with multilayer delaminations using wavenumber analysis and their sensitivity to the delamination severity are very limited.

This article presents a numerical and experimental investigation on the detection and characterization of multilayer delaminations in carbon fiber–reinforced polymer (CFRP) composite plates using guided waves and wavenumber analysis. First, a 3-mm in-house quasi-isotropic $[-45/90/45/0]_{3s}$ CFRP composite plate with purpose-built delaminations by inserting Teflon films was manufactured, and the ultrasonic C-scan was conducted to verify and image the simulated multilayer
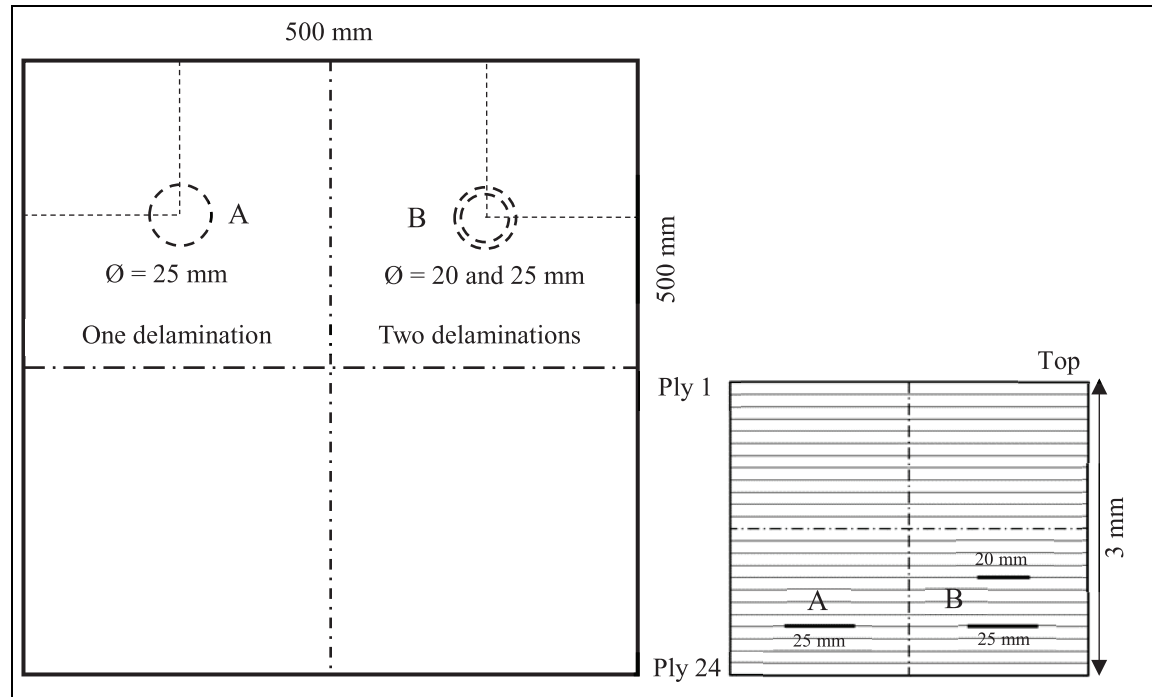
Figure 1. Schematic of 3-mm thick quasi-isotropic $[-45/90/45/0]_{3s}$ carbon fiber–reinforced polymer (CFRP) composite plate with one delamination and two delaminations.

delaminations including one delamination and two delaminations. Then, multiphysics 3D FE simulations of the composite plate with five different delamination scenarios using the commercial ANSYS FE software were carried out to study guided wave interaction with delaminations, especially the trapped waves due to the multilayer delaminations. Next, experimental validations using SLDV measurements were conducted to measure out-of-plane wave motion on the composite plate with one delamination and two delaminations. Wavenumber analysis was used to study guided wave interactions with delaminates in order to better understand the complex behavior that occurs when waves encounter multilayer delaminations. Finally, for proof of concept, a pitch–catch experiment using angle beam transducers is carried out as a suggestion for practical implementations to detect and separate one and two delaminations. Both numerical and experimental results demonstrate a good capability for the detection and characterization of multilayer delaminations in composite structures.

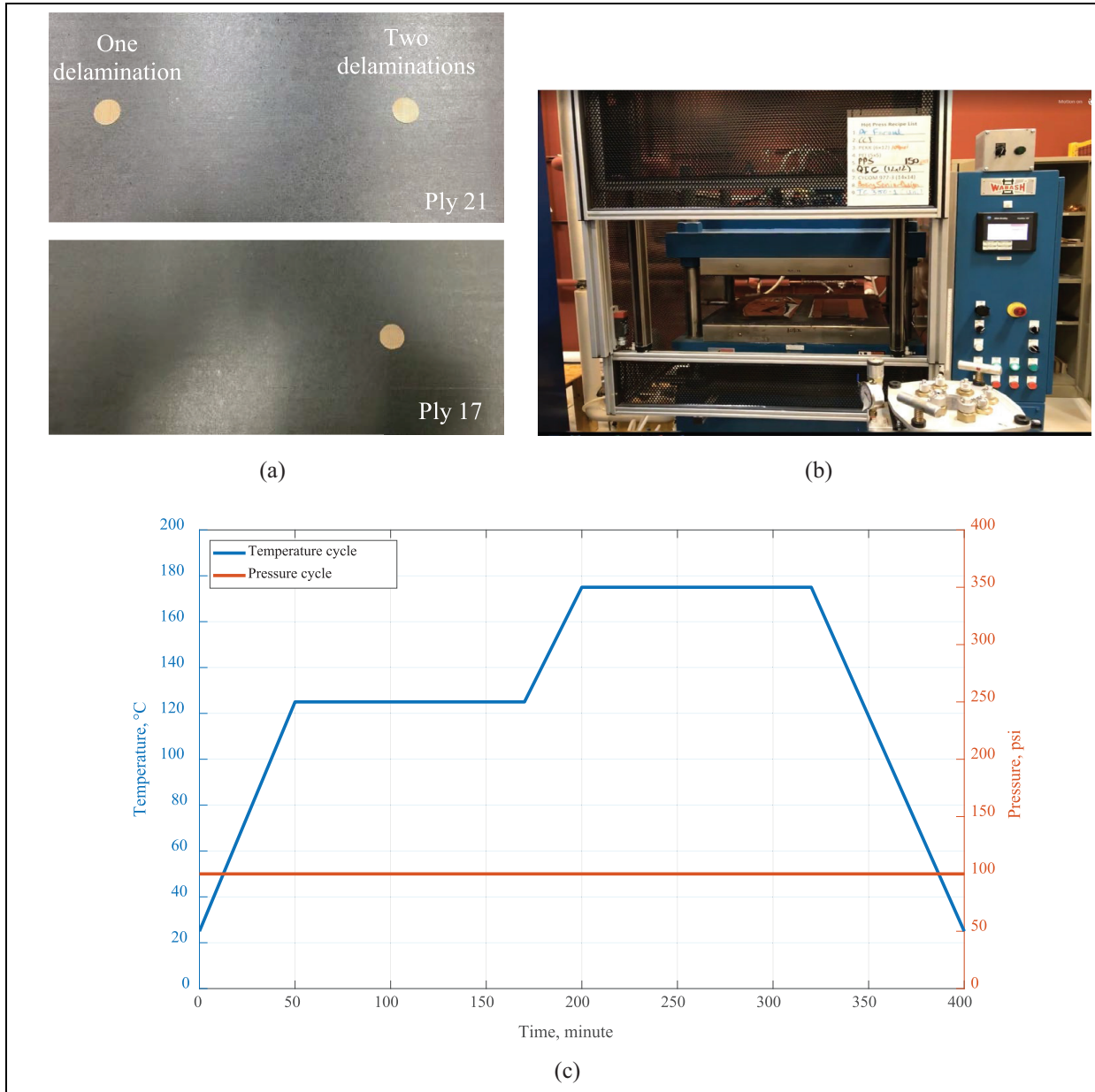## Composite specimen

Simulated multilayer delaminations

In this study, a 3-mm thick in-house quasi-isotropic CFRP composite plate with a stacking sequence of $[-45/90/45/0]_{3s}$ was investigated. The IM7 12K/

CYCOM 5320-1 prepreg was used to manufacture the composite specimen. Two different delamination scenarios—one and two delaminations—were generated by inserting Teflon films during the ply layup process.

Figure 1 shows the schematic of the 3-mm thick quasi-isotropic CFRP composite plate with purpose-built multilayer delaminations. One delamination was created by inserting a circular Teflon film (25 mm in diameter) between plies 20 and 21. Two delaminations were generated by inserting two Teflon films of different sizes at various depths. First, a large circular Teflon film (25 mm in diameter) was inserted between plies 20 and 21, which is the same size and depth of one delamination. Then, an additional small circular Teflon film (20 mm in diameter) was inserted between plies 16 and 17. The thickness of Teflon film is 50 microns. The depth of the Teflon insert was based on the experimental results in Wallentine and Uchic.[11] The delamination size was determined from the practical application, where the critical delamination size for growth monitoring is around 25 mm diameter. After the ply layup, the specimen was placed in a hot press machine for curing. The experimental setup and curing cycle of specimen manufacturing are given in Figure 2.

Ultrasonic non-destructive inspection

Ultrasonic non-destructive testing (NDT) was conducted to verify and image the simulated delaminations

Figure 2. Experimental setup and curing cycle of the specimen manufacturing: (a) Teflon inserts, (b) hot press machine, and (c) curing cycle.

in the quasi-isotropic CFRP composite plate. An ultrasonic immersion tank was used to inspect the specimen. In the experiment, a 10 MHz, 25.4-mm focused transducer was utilized. First, a full specimen inspection was performed, and it was found that there were no manufacturing defects other than the simulated delaminations. Then, small-area C-scans were conducted to verify and image the simulated delaminations. The scan area is 100 mm × 100 mm. Figure 3(a) shows the ultrasonic C-scan results of the pristine area. It can be found that no manufacturing defects and the quasi-isotropic layup were observed. Figure 3(b) and (c) gives the

C-scan results of one delamination. In this case, ultrasonic C-scans were conducted on both bottom surface (bottom scan) and top surface (top scan). It can be seen that one 25-mm delamination was clearly noted from both bottom and top scans. From the C-scan images, the size and shape of the delamination can be clearly observed.

The NDT inspection results of two delaminations are shown in Figure 4. First, the ultrasonic C-scan was conducted on the bottom surface which is close to the large 25-mm delamination. Figure 4(a) shows the C-scan result of the bottom scan. It can be found that
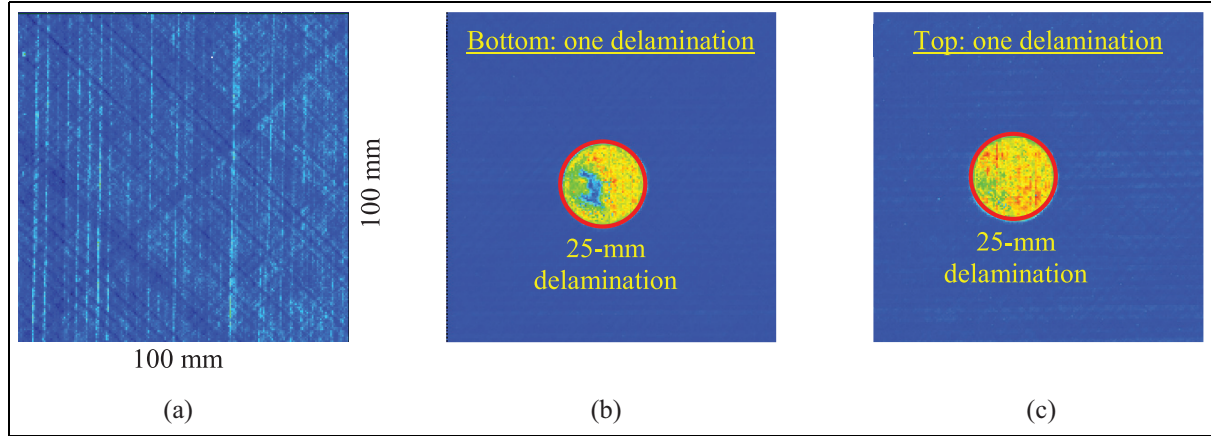
Figure 3. NDT ultrasonic C-scan results: (a) pristine area, (b) bottom scan of one delamination, and (c) top scan of one delamination.
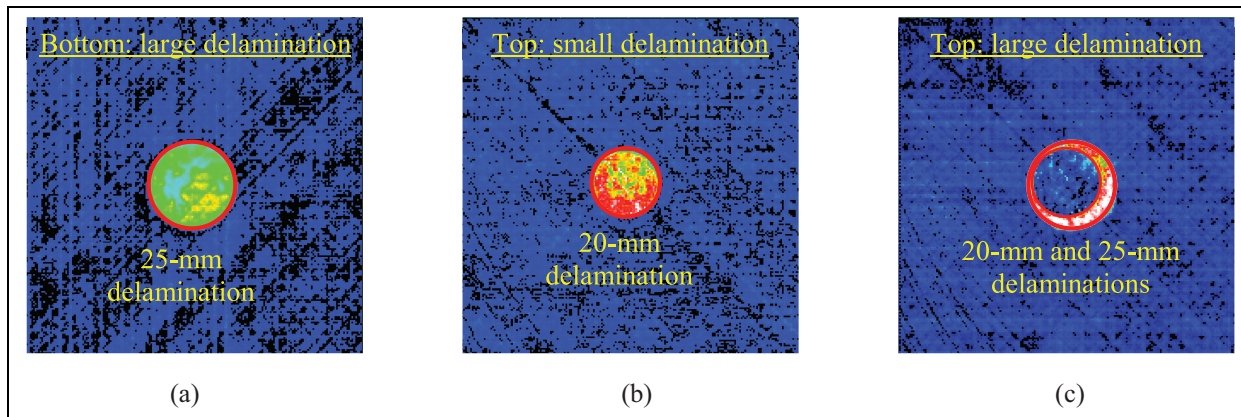
Figure 4. Ultrasonic NDT inspection results of two delaminations: (a) bottom scan showing 25-mm delamination, (b) top scan showing 20-mm delamination, and (c) top scan showing 20-mm and 25-mm delaminations.

only a 25-mm delamination was observed because the large delamination is close to the bottom surface, which blocks all the ultrasonic waves to penetrate. Therefore, the hidden small delamination cannot be detected from the bottom surface and this may happen in the practical applications when only single-sided access is available.

In order to detect the small delamination, the top scan with different focusing was performed. First, a 20-mm delamination was noted in Figure 4(b) when the focus was conducted at the depth of the small delamination, while a 25-mm delamination was also observed when the focus was performed at the depth of the large delamination as shown in Figure 4(c). A 20-mm shadow was clearly observed in Figure 4(c), which is the small delamination at a different depth, and it blocks the ultrasonic wave to penetrate. Therefore, the simulated multilayer delaminations were successfully detected and quantified from the ultrasonic NDT detection, which is consistent with the design.

Guided waves in the composites

Measurement of material properties

The material properties of the in-house composite plate were measured experimentally using the ultrasonic immersion technique proposed in Barazanchy et al.[45] The retrieved engineering elastic constants are given in Table 1. To validate the retrieved material properties, a comparison between the experimental frequency–wavenumber dispersion curve and the theoretical dispersion curve was conducted. In this experiment, the time-space guided wave data were obtained from the SLDV line scan in the 0° direction on the pristine area. The quantity measured by the SLDV is the out-of-plane velocity of surface particle motion. The excitation signal applied to the PWAS transducer is a linear sine wave chirp from 50 to 900 kHz.

To obtain the frequency–wavenumber dispersion curves, the measured time-space data $u(t, x)$ were

Table 1. Engineering constants of the unidirectional prepreg.

E_{11}	E_{22}	E_{33}	ν_{12}	ν_{13}	ν_{23}	G_{12}	G_{13}	G_{23}	ρ
153 GPa	8.7 GPa	8.7 GPa	0.37	0.37	0.5	6.9 GPa	6.9 GPa	2.9 GPa	1625 kg/m³
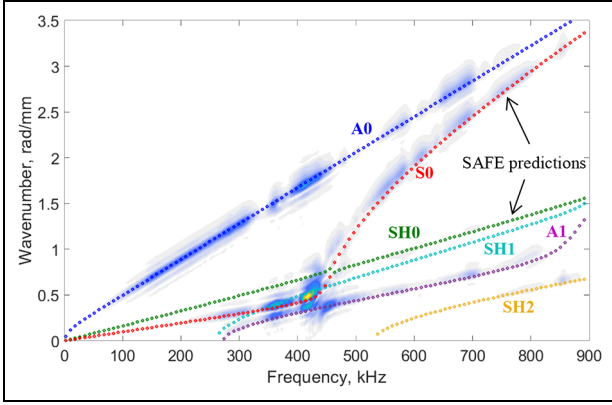
Figure 5. Comparison between experimental and theoretical frequency–wavenumber dispersion curves in the 0° direction.

transformed into the frequency–wavenumber domain by applying a 2D fast Fourier transform (FFT)[46]

$$U(f, \xi) = \int_{-\infty}^{\infty} \int_{-\infty}^{\infty} u(t, x) e^{-i(\xi x - 2\pi f t)} dt dx \quad (1)$$

where $U(f, \xi)$ is the experimental frequency–wavenumber representation in terms of the frequency variable f and the wavenumber variable ξ.

The theoretical frequency–wavenumber dispersion curve was calculated using the measured material properties and the SAFE approach.[7] For the SAFE approach, 48 one-dimensional (1D) quadratic elements across the thickness direction were utilized to ensure the convergence of the solution. The comparison between experimental and theoretical frequency–wavenumber dispersion curves in the 0° direction is shown in Figure 5. The dotted lines are the theoretical frequency–wavenumber dispersion curves for all the wave modes in the quasi-isotropic CFRP composite plate. A good match between the experiment and the prediction of measured material properties was achieved. Besides the fundamental A0, S0, and SH0 modes, high-order modes such as A1, SH1, and SH2 were successfully generated in the 3-mm quasi-isotropic composite plate. It can be found that the A0 mode has a strong out-of-plane velocity at low frequency (below 250 kHz).

Prediction of dispersion curves in the composite plate

In this section, the SAFE approach was used to calculate the dispersion curves in the quasi-isotropic composite plate based on the retrieved material properties. Figure 6(a) presents the phase velocity curves in the 0° direction. It can be noted that at relatively low frequency, only three fundamental wave modes (S0, SH0, and A0) exist. The S0 mode is not very dispersive at the frequency below 300 kHz and S0 mode has a large phase velocity. The A0 mode, however, is highly dispersive and has the lowest phase velocity. The SH0 mode is mildly dispersive at the frequency below 400 kHz and possesses a phase velocity between A0 and S0. Figure 6(b) shows the phase velocity curves in the 90° direction. It should be noted that, compared with the results in the 0° direction, S0 mode, SH0 mode, and A0 mode do not change much at the frequency below 400 kHz because the specimen investigated is a quasi-isotropic composite. However, obvious differences are observed for high-order modes at the frequency above 400 kHz.
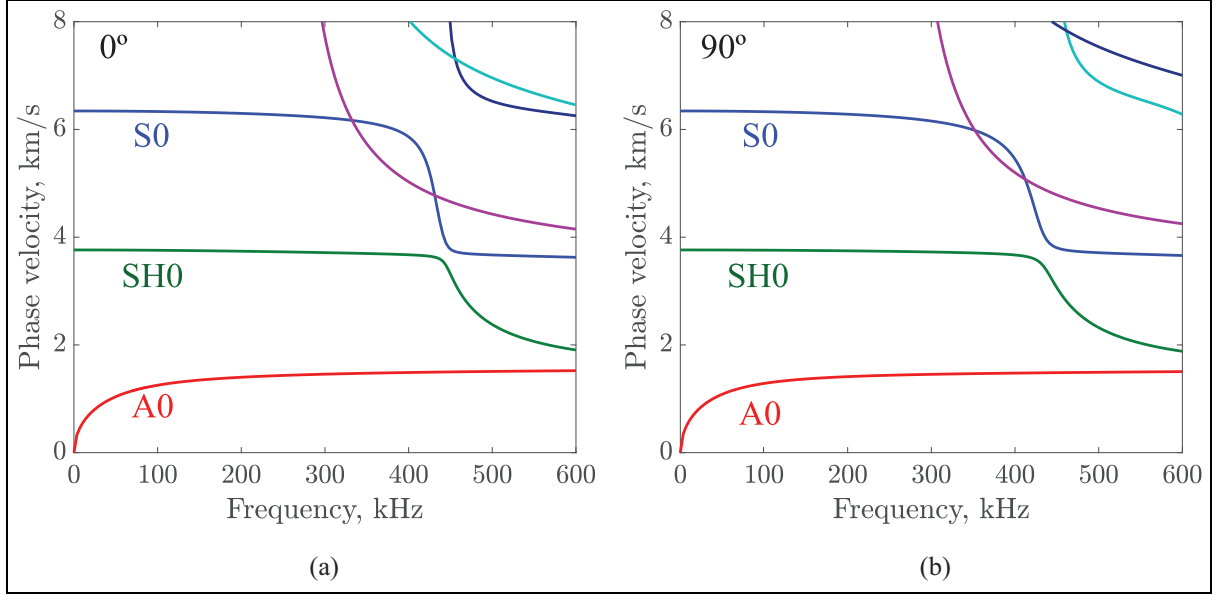
Figure 7 shows the group-velocity directivity plot at 200 kHz. The curves represent the spatial wave propagation pattern. It can be observed that all the three wave modes, S0, SH0, and A0, have similar group velocities in all directions. This is because the quasi-isotropic composite plate has similar material properties in various directions. Thus, if the waves are excited by a point source, then a quasi-circular wave crest would be obtained.

Multiphysics FE simulation

3D multiphysics FE models were utilized to simulate guided wave propagation and interaction with different delamination scenarios—one delamination, two delaminations, three delaminations, four delaminations, and five delaminations—in the 3-mm thick $[-45/90/45/0]_{3s}$ CFRP composite plate.

Delamination modeling

Six sets of 3D simulations were carried out to characterize multiple delaminations: (1) 3D wave propagation in the pristine plate, (2) 3D wave propagation in the damaged plate with one delamination, (3) 3D wave propagation in the damaged plate with two delaminations, (4) 3D wave propagation in the damaged plate

Figure 6. Phase-velocity dispersion curves in the 3-mm quasi-isotropic CFRP composite plate: (a) 0° and (b) 90°.
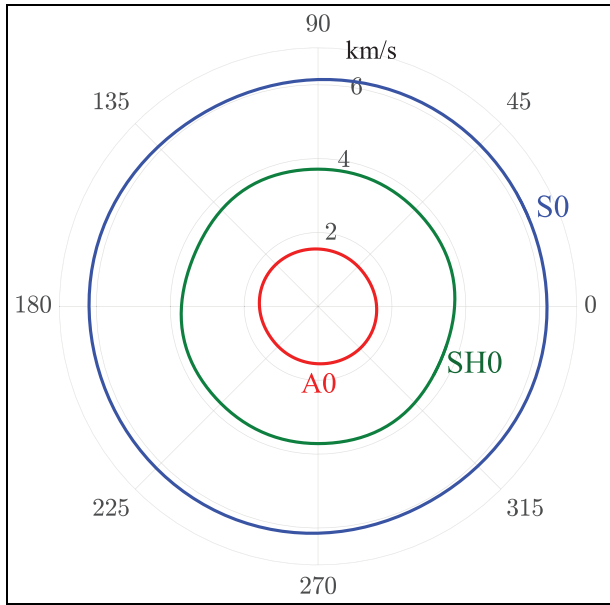
**Figure 7.** Group-velocity directivity curves at 200 kHz in the 3-mm quasi-isotropic CFRP composite plate.

with three delaminations, (5) 3D wave propagation in the damaged plate with four delaminations, and (6) 3D wave propagation in the damaged plate with five delaminations. Figure 8 shows the FE models of the quasi-isotropic CFRP composite plate with five different delamination cases. In this study, the delaminations were modeled by detaching the nodes, which have been widely used by many authors Tian et al.[20] and Ramadas et al.[36,37] The number of delaminations is increased from one to five to study the guided wave interactions with various multilayer delaminations. For the case of one delamination, a 25-mm delamination is created between plies 20 and 21 by specifying the delamination as two planes, which are defined by the same coordinates but are not tied together. For the case of two delaminations, a 25-mm delamination between plies 20 and 21 and a 20-mm delamination between plies 16 and 17 are generated. One more 16-mm delamination between plies 11 and 12 is introduced for the case of three delaminations based on two delaminations. For the case of four delaminations, an additional 13-mm delamination between plies 7 and 8 is added based on three delaminations. Finally, one more 10-mm delamination between plies 3 and 4 is introduced for the case of five delaminations, as shown in Figure 8. These delamination depths were chosen based on the experimental results in Wallentine and Uchic.[11]

The PZT-5A material properties are assigned to the PWAS transducer as follows

$$[C_p] = \begin{bmatrix} 120.2 & 75.1 & 75 & 0 & 0 & 0 \\ 75.1 & 120.2 & 75 & 0 & 0 & 0 \\ 75 & 75 & 110.7 & 0 & 0 & 0 \\ 0 & 0 & 0 & 21.1 & 0 & 0 \\ 0 & 0 & 0 & 0 & 21.1 & 0 \\ 0 & 0 & 0 & 0 & 0 & 22.6 \end{bmatrix} \text{GPa} \tag{2}$$

$$[\varepsilon_p] = \begin{bmatrix} 918 & 0 & 0 \\ 0 & 918 & 0 \\ 0 & 0 & 827 \end{bmatrix} \times 10^{-8} \text{F/m} \tag{3}$$
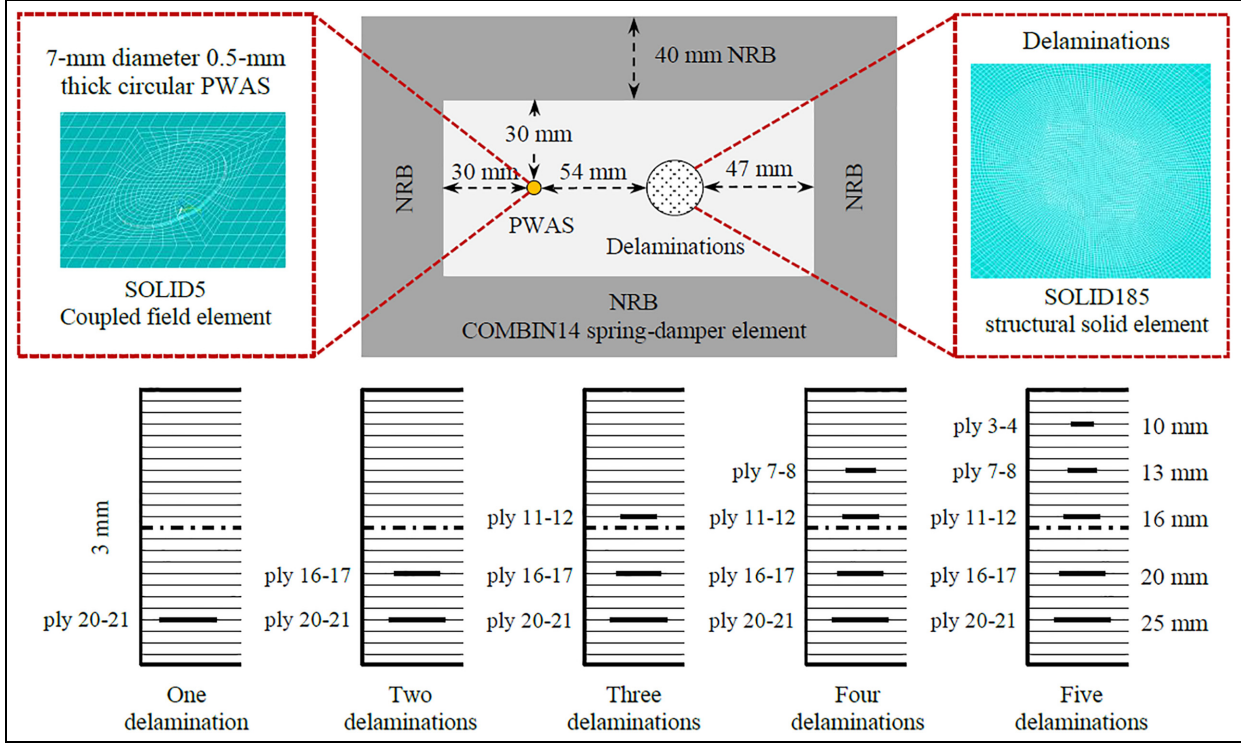
Figure 8. Multiphysics finite element model of the quasi-isotropic composite plate with five different delamination cases.

$$[e_p] = \begin{bmatrix} 0 & 0 & 0 & 0 & 12.29 & 0 \\ 0 & 0 & 0 & 12.29 & 0 & 0 \\ -5.35 & -5.35 & 15.78 & 0 & 0 & 0 \end{bmatrix} C/m^2$$

(4)

where $[C_p]$ is the stiffness matrix, $[\varepsilon_p]$ is the dielectric matrix, and $[e_p]$ is the piezoelectric matrix. The density of the PWAS material is 7800 kg/m^3.

Non-reflective boundaries (NRB) developed by Shen and Giurgiutiu[47] can eliminate boundary reflections, and thus allow for the simulation of guided wave propagation in an infinite medium with small-size models. This NRB was implemented around the 3D FE models to calculate the transient response under the PWAS excitation. The PWAS transducer was modeled with coupled field elements (SOLID5) in the commercial FE package ANSYS 17. Structural solid elements (SOLID185) were used to mesh the composite plate. COMBIN14 spring-damper elements were utilized to construct the NRB. A Rayleigh damping ($\beta = 3 \times 10^{-8}$) was considered to simulate the damping effect of the composite material. The damping value was determined by iterative calibration to match the experimentally measured attenuation coefficient.

In this study, the excitation signal is a three-count Hanning window modulated tone burst with the center frequency of 200 kHz, which is in the less dispersive region. A0 mode at 200 kHz has a dominant out-of-plane wave motion as shown in Figure 5. Besides, A0 mode has a short wavelength, which is sensitive to small-size delaminations. The mesh size adopted in this study was 0.5 mm for in-plane direction to guarantee that more than 20 elements exist per wavelength and 0.125 mm for the thickness direction to ensure one element per ply. The PWAS transducer and delamination regions were meshed with even finer elements to accommodate the high-stress gradient. The time step was set to 0.25 μs to ensure convergence.

Simulation results

First, the out-of-plane velocity on the top surface was extracted and visualized to study the guided wave interaction with the multiple delaminations. Figure 9 shows the comparison of the transient spatial wavefields among the pristine plate and the damaged plate with five various delamination cases.

For the pristine case in Figure 9(a), it can be found that a quasi-circular wavefront was generated because of the quasi-isotropic stacking sequence used for this CFRP composite plate, strong near the wave source and weak at the far field due to the outward propagation pattern. At 25 μs, the fast propagating S0 mode with a long wavelength and lower amplitude and the
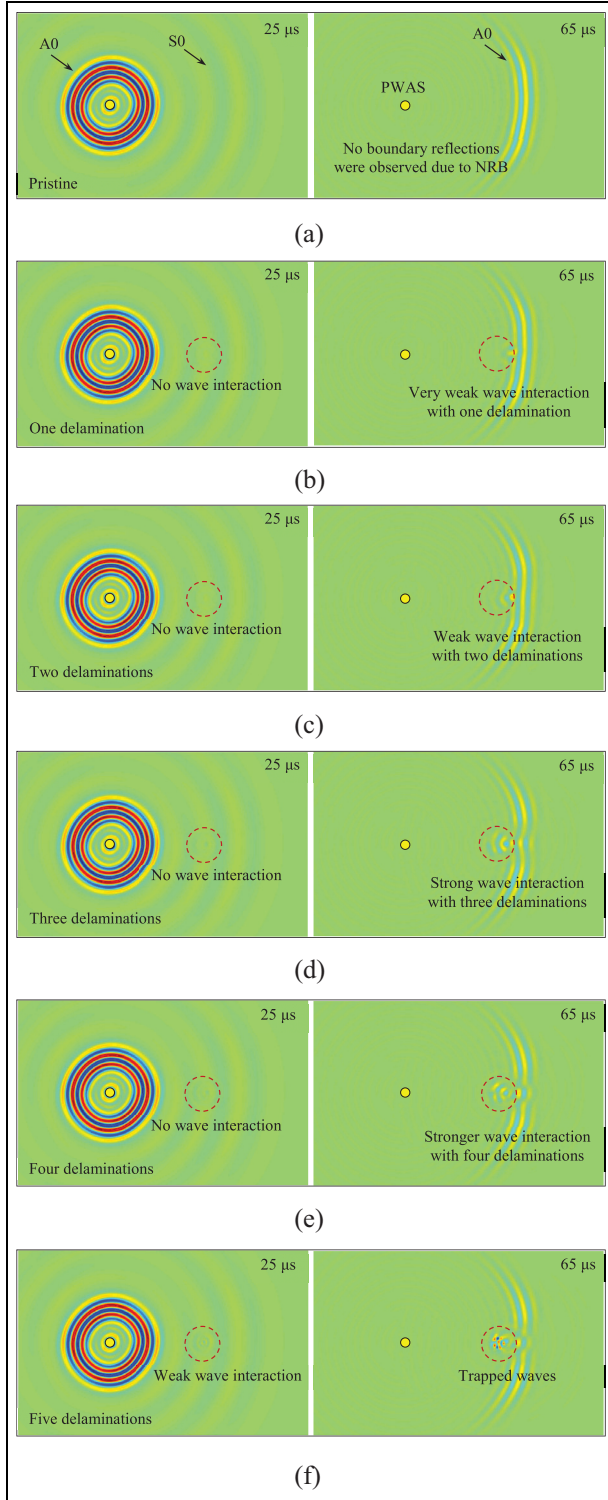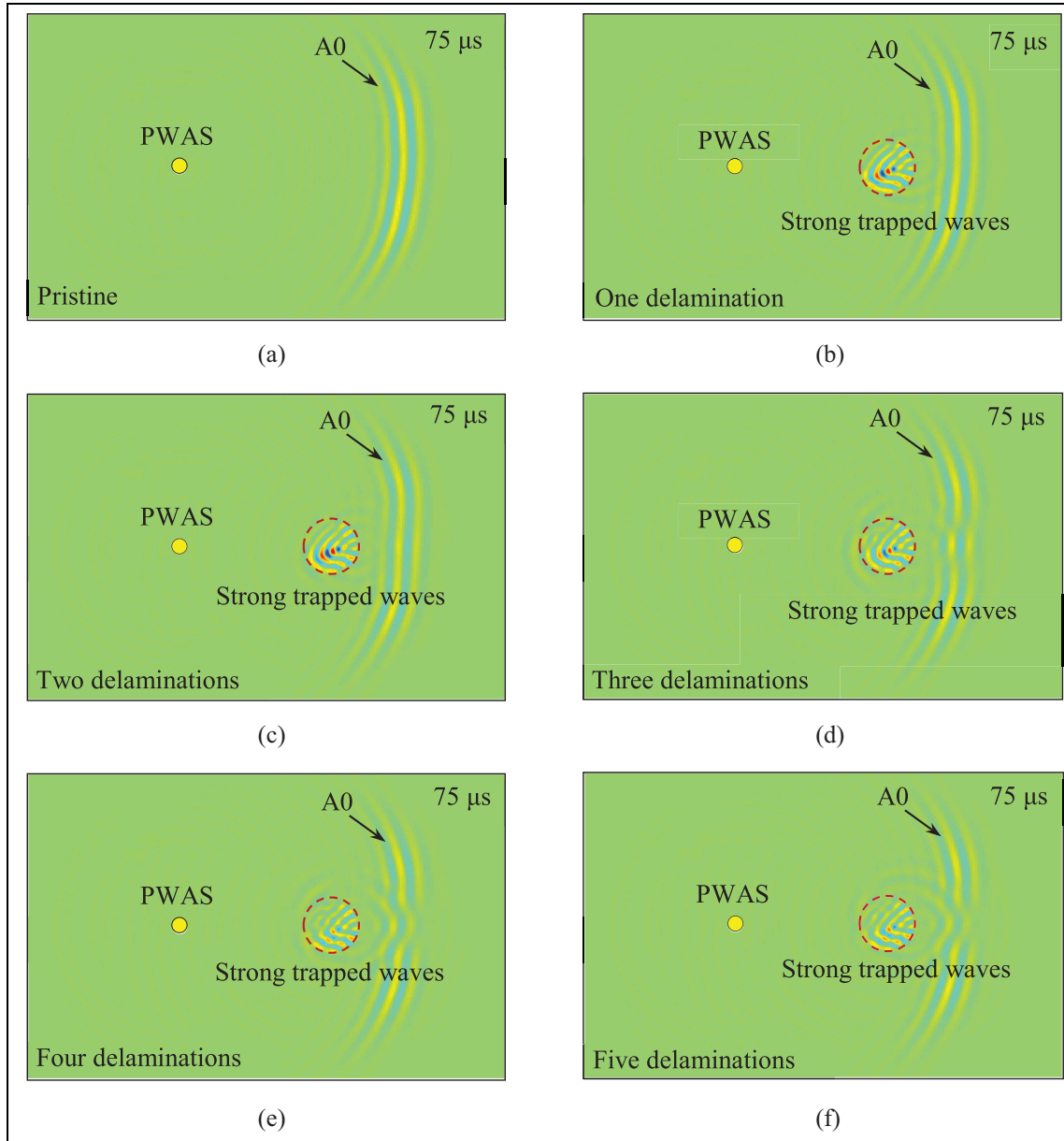
Figure 9. Comparison of the transient spatial wavefield in the composite plate showing the out-of-plane velocity on the top surface: (a) pristine plate, (b) one delamination, (c) two delaminations, (d) three delaminations, (e) four delaminations, and (f) five delaminations.

slowly propagating A0 mode with a short wavelength and higher amplitude can be clearly identified. At 65 μs, the incident waves were successfully absorbed by NRB and no reflections occurred. Figure 9(b) to (e) shows the guided wave propagation and interaction with one, two, three, and four delaminations, respectively. At 25 μs, no obvious S0 interaction with the delaminations can be identified. At 65 μs, the A0 wave interactions with the delaminations became stronger when the number of delaminations increased. This is because the newly added delamination is close to the top surface as shown in Figure 8. The wave interaction with five delaminations is given in Figure 9(f). It was found that strong trapped waves were noted within the 10-mm delamination region after A0 interacted with the delaminations.

Second, the guided wavefield on the bottom surface was investigated. Figure 10 shows the comparison of the transient spatial wavefield on the bottom surface of the 3-mm quasi-isotropic composite plate. Figure 10(a) presents the guided wave propagation in the pristine plate. Similar to the results on the top surface, the strong A0 mode with a short wavelength was clearly observed. Figure 10(b) to (f) shows the guided wave propagation and interaction with five different delamination cases on the bottom surface. At 75 μs, after A0 waves interact with the delaminations, strong trapped waves in the delamination regions can be observed for five different delamination cases. This is because the largest 25-mm delamination is close to the bottom surface for all the scenarios, as shown in Figure 8. Previous studies have confirmed the multiple reflections within the delamination area and a considerable amount of ultrasonic energy is trapped in the delaminated region. The observed behavior agrees well with the wavefield observations presented in Tian et al.[20] However, various multiple delaminations cannot be characterized by directly comparing the guided wavefield.

Wavenumber analysis

To further analyze the wave interaction with multilayer delaminations, line scans across the delamination areas on the top and bottom surfaces were extracted from the simulation results. Figure 11(a) to (e) shows the time-space wavefields of the out-of-plane velocity on the top and bottom surfaces for the cases of one delamination, two delaminations, three delaminations, four delaminations, and five delaminations, respectively. As it can be seen, the out-of-plane velocity of A0 mode has a higher amplitude than the S0 mode.

Figure 10. Comparison of the transient spatial wavefield in the composite plate showing the out-of-plane velocity on the bottom surface: (a) pristine plate, (b) one delamination, (c) two delaminations, (d) three delaminations, (e) four delaminations, and (f) five delaminations.

For the results on the top surface, it was found that wave interaction became stronger when the number of delaminations increased from one to five. This is because the newly added delaminations are close to the top surface. These phenomena may be used to indicate delamination severity. Similarly, a higher amplitude but slower A0 mode and a lower amplitude but faster S0 mode were observed from the time-space wavefields of out-of-plane velocity on the bottom surfaces for all the delamination cases. Comparing with the wavefield on the top surface, it can be found that the strong trapped

waves within the delamination regions were observed on the bottom surface. However, slight differences were noted for all the delamination cases. Therefore, it is difficult to distinguish the various delamination cases by analyzing the wavefield on the bottom surface because the dominant wave interaction occurs at the largest 25-mm delamination near the bottom surface.

Although wave interactions with the delamination and the boundaries are visualized in the time-space wavefield, implicit wave propagation characteristics such as wave mode content and how modes change
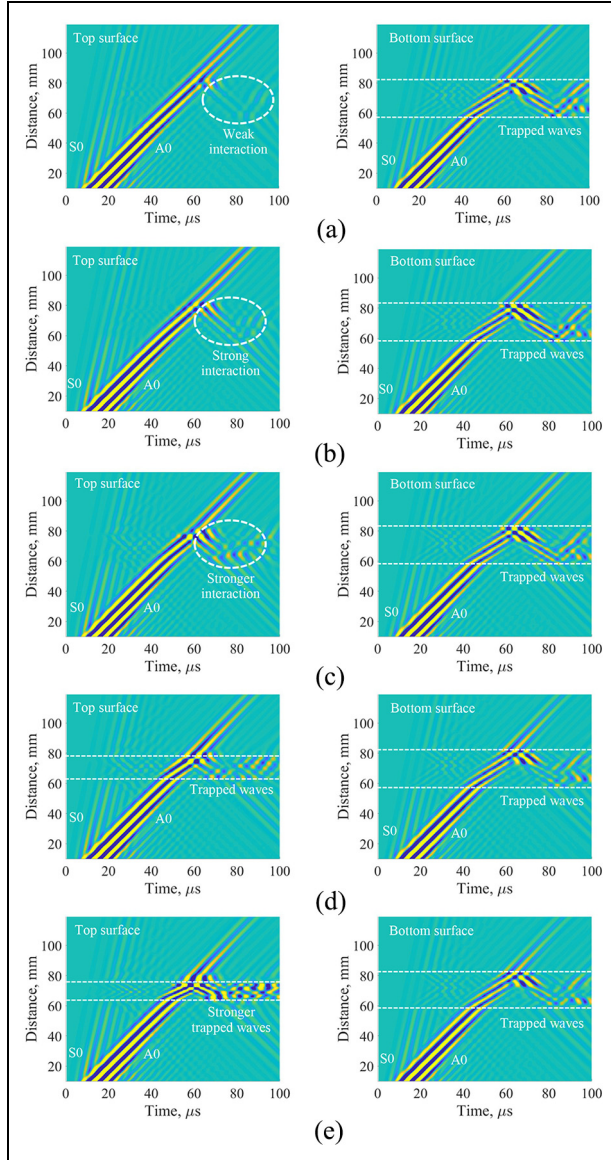
Figure 11. Comparison of FEM time-space wavefield on the top surface and the bottom surface: (a) one delamination, (b) two delaminations, (c) three delaminations, (d) four delaminations, and (e) five delaminations.

along the wave propagation path are not readily seen. It has been demonstrated that wavenumber analysis representing the wavenumber content has abundant information regarding the existence of various wave modes and wave propagation characteristics.[20] Therefore, the time-space wavefield was transformed into frequency–wavenumber representation using 2D FFT.

Wavenumber analysis of full wavefield. First, the wavenumber analysis of one and two delaminations using the full

wavefield was conducted. Figure 12 shows the comparison of frequency–wavenumber spectrums on the top surface between one and two delaminations. The black and red solid lines are the theoretical dispersion curves of A0 mode and S0 mode in the quasi-isotropic CFRP composite plate, respectively. It can be found that strong incident A0 mode (positive wavenumber) was observed in the frequency–wavenumber spectrums, which agrees well with the theoretical dispersion curves. Compared with the result of one delamination, it was found that a stronger negative wavenumber (backward propagation) was clearly observed for the case of two delaminations, which demonstrates that the more delamination, the stronger reflections.

Figure 13 shows the comparison of frequency–wavenumber spectrums using full wavefield on the bottom surface between one and two delaminations. It can be found that new wavenumber components including both positive (forward propagation) and negative (backward propagation) due to the delaminations can be clearly observed. It is expected that the new wavenumber components are related to the wave propagation in the delamination regions. The meaning of the new wavenumber was further investigated to better understand the trapped waves in the delamination regions. Unlike conventional guided wave methods which only determine the delamination location in the plate, wavenumber analysis will identify the ply below which the delamination occurs.[20] This is because the sublaminates above or below the delaminations will have different layups and thicknesses compared to the pristine composite plate. The propagation characteristics and wavenumbers would be modified due to the thickness and layup change.

The depth of delamination was estimated by fitting the newly wavenumber components with the theoretical dispersion curves of the sublaminates due to the delamination. Theoretical dispersion curves of the sublaminates were calculated using the ply-level material properties and layup. For example, the layups of bottom four layers and eight layers for this specific specimen are [−45/90/45/0] and [−45/90/45/0/−45/90/45/0], respectively. From the wavenumber spectrum of one delamination, it can be found that the new frequency–wavenumber components are mainly related to the A0 mode in the bottom four [−45/90/45/0] layers. Therefore, the delamination depth can be estimated above the bottom fourth ply. For the case of two delaminations, strong new negative wavenumber due to the trapped waves in the delamination regions was observed when an additional delamination exists, which indicates that the more delaminations in the composite, the stronger wave energy was trapped. However, the new frequency–wavenumber components corresponding to the bottom eight layers were hardly
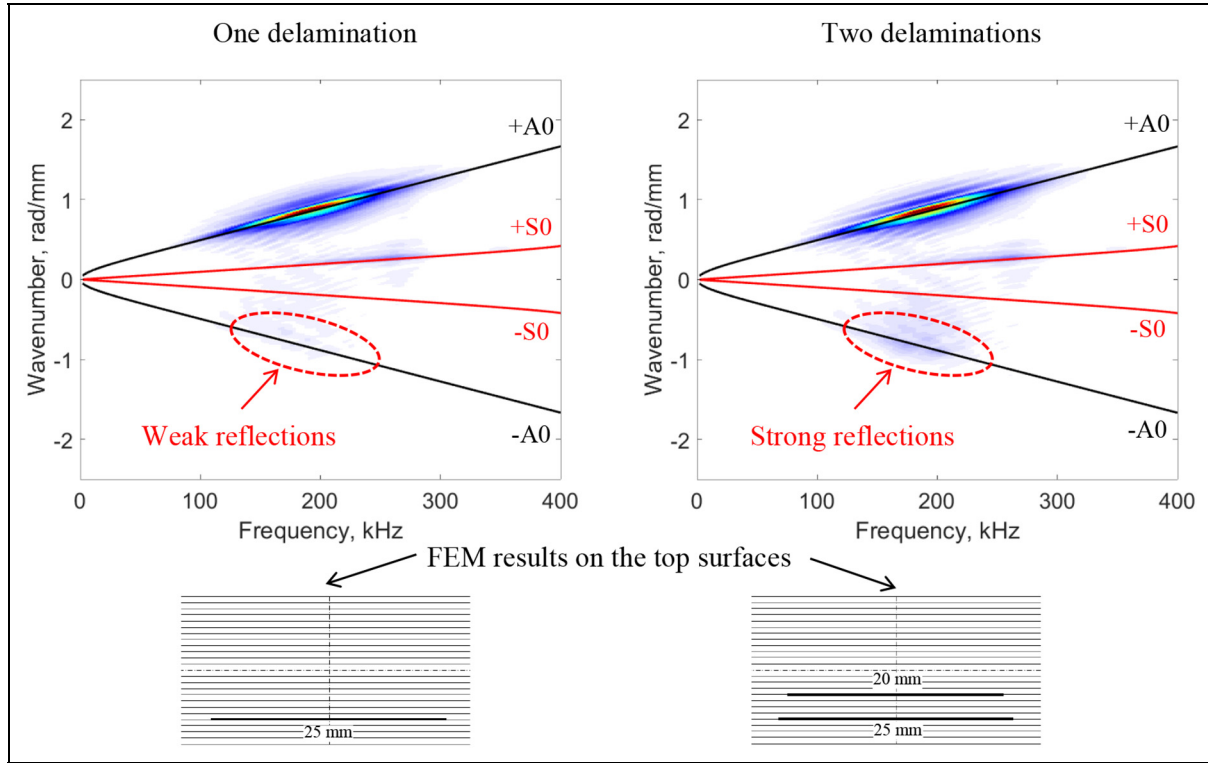
Figure 12. Comparison of FEM frequency–wavenumber spectrums on the top surface between one delamination and two delaminations.
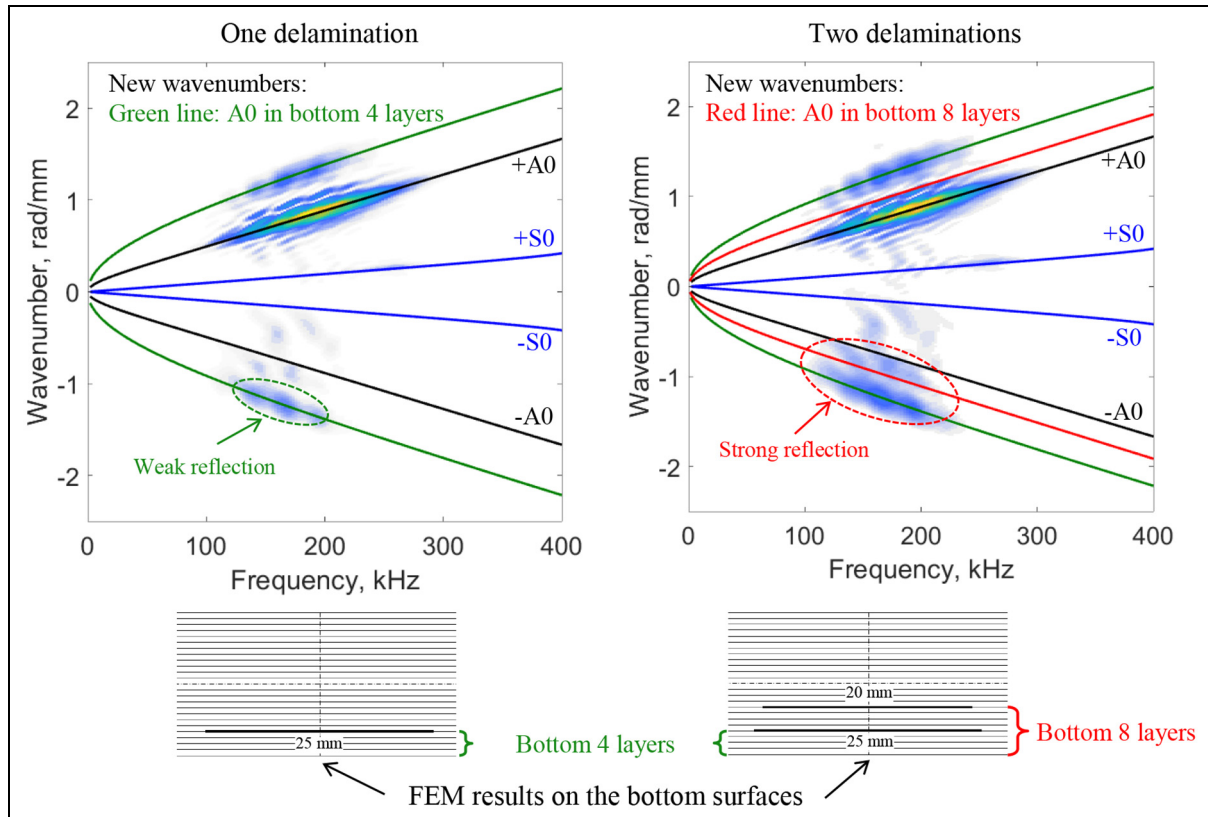
Figure 13. Comparison of FEM frequency–wavenumber spectrums on the bottom surface between one delamination and two delaminations.

observed for the case of two delaminations because the trapped waves observed mainly came from the wave interaction with the largest 25-mm delamination near the bottom surface.

Wavenumber analysis of windowed delamination wavefield. In this section, a windowed delamination wavefield was used for wavenumber analysis to characterize the multiple delaminations, which is the time-space wavefield in the delamination region from 57.5 to 82.5 mm, as shown in Figure 11. Figure 14 shows the frequency–wavenumber spectrums of the windowed wavefields on the top surface for five various delamination cases. The five different delamination cases can be distinguished based on the various frequency–wavenumber spectrums. It was found that the positive wavenumbers match well the theoretical wavenumber in the sublaminates above the delaminations. Therefore, the dominant A0 wavenumber was identified from the top sublaminate of delamination near the top surface. Figure 14(a) and (b) shows the spectrums of one delamination and two delaminations. It was found that stronger negative new wavenumbers were observed when the number of delaminations increased from one to two.

Figure 15 shows the frequency–wavenumber spectrums of the windowed wavefields on the bottom surface for five delamination cases. First, a large difference in the new negative wavenumber was noted for various delamination cases. The positive wavenumbers agree well with the theoretical A0 wavenumber in the sublaminate of bottom four layers. This is because the largest 25-mm delamination is close to the bottom surface, where the dominant wave–delamination interaction occurs. For the cases of one delamination and two delaminations, it was found that stronger negative new wavenumbers were observed when the number of delaminations increased from one to two, which is consistent with the results on the top surface.

The study in this section has confirmed that as waves propagate through a delamination region and they can be trapped in the delamination, generating new wavenumbers. These new wavenumbers measured on the composite surface close to the delamination can be used to detect the delamination depth.

Discussion of delamination ply depth detection. In this study, the delamination ply depth detection is achieved by fitting new wavenumbers obtained from theoretical wavenumber dispersion of assumed sublaminates and comparing it with the observed frequency–wavenumber spectrum. However, the accuracy of this method depends on the new wavenumber difference in sublaminates.

Figure 16(a) shows the theoretical dispersion curves of A0 mode in the sublaminates of bottom six plies, eight plies, and ten plies, respectively. At the excitation frequency of 200 kHz, a large wavenumber difference was observed in sublaminates of bottom six plies and eight plies, as shown in Figure 16(b). Therefore, it is easy to distinguish the delamination occurring above the bottom eighth ply and bottom sixth ply. However, a slight difference was noted in sublaminates of bottom eight plies and ten plies, which challenges the estimation of delamination occurring above bottom eighth ply and bottom tenth ply. To improve the estimation in this scenario, a higher excitation frequency would be utilized. Because the wavenumber difference increases with the frequency and it will be more sensitive to the delamination location.

### Scattering directivity patterns of multilayer delaminations

To further investigate the sensitivity of guided waves to delamination severity, the scattering directivity patterns were obtained by determining the maximum absolute amplitude of the scattered waves, which are the differences between pristine signals and damaged signals along a circular line as shown in Figure 17.

By extracting simulation signals along a circular line on the composite plate with and without delaminations, the scattered waves generated from the guided wave interaction with the multilayer delaminations can be determined and separated from the incident waves by

$$v_z^S(r, \theta, t) = v_z^D(r, \theta, t) - v_z^P(r, \theta, t) \tag{5}$$

where $v_z^D(r, \theta, t)$ and $v_z^P(r, \theta, t)$ are the FEM out-of-plane velocity of guided waves at location (r, θ) for the composite plate with and without delamination, respectively. $v_z^S(r, \theta, t)$ is the out-of-plane velocity of the scattered waves from the multilayer delaminations. r and θ are the radial and azimuthal coordinates of the cylindrical coordinate system shown in Figure 17.

For determining the scattering directivity pattern of the delaminations, the out-of-plane velocities of 180 points at $r = 25$ mm and $0° \leqslant \theta \leqslant 360°$ with $2°$ step increments were collected for both the pristine plate and the damaged plate with five different delamination cases. The scattering directivity pattern was obtained by determining the maximum absolute amplitude of the scattered waves using equation (5) in the time domain. It should be noted that all scattering amplitudes are normalized by the maximum absolute amplitude of the incident wave at the delamination center location of the pristine plate. As a representative, Figure 18 presents the comparison of the scattered waves between one and two delaminations in the forward direction
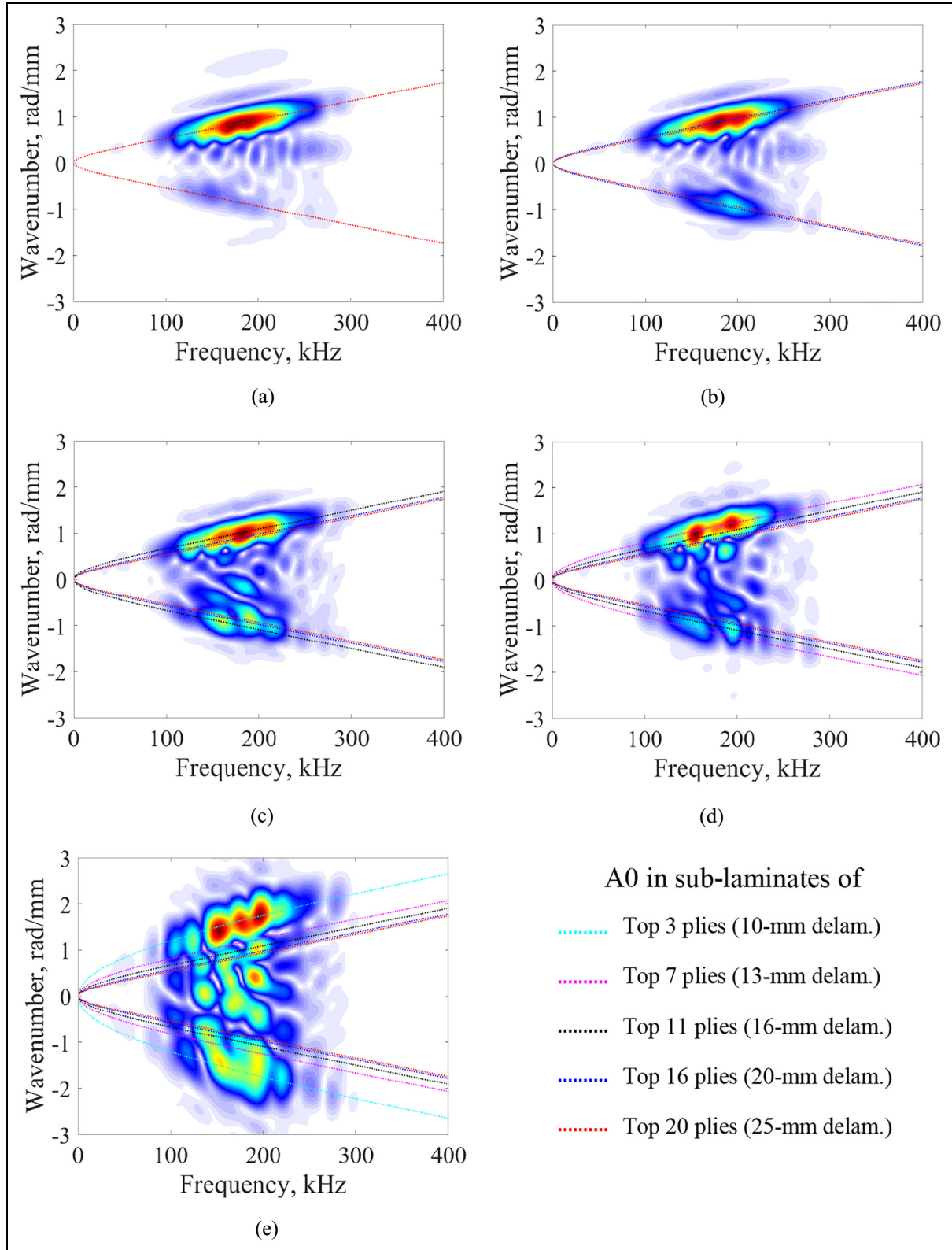
Figure 14. Frequency–wavenumber spectrums of the windowed wavefields on the top surface: (a) one delamination, (b) two delaminations, (c) three delaminations, (d) four delaminations, and (e) five delaminations.
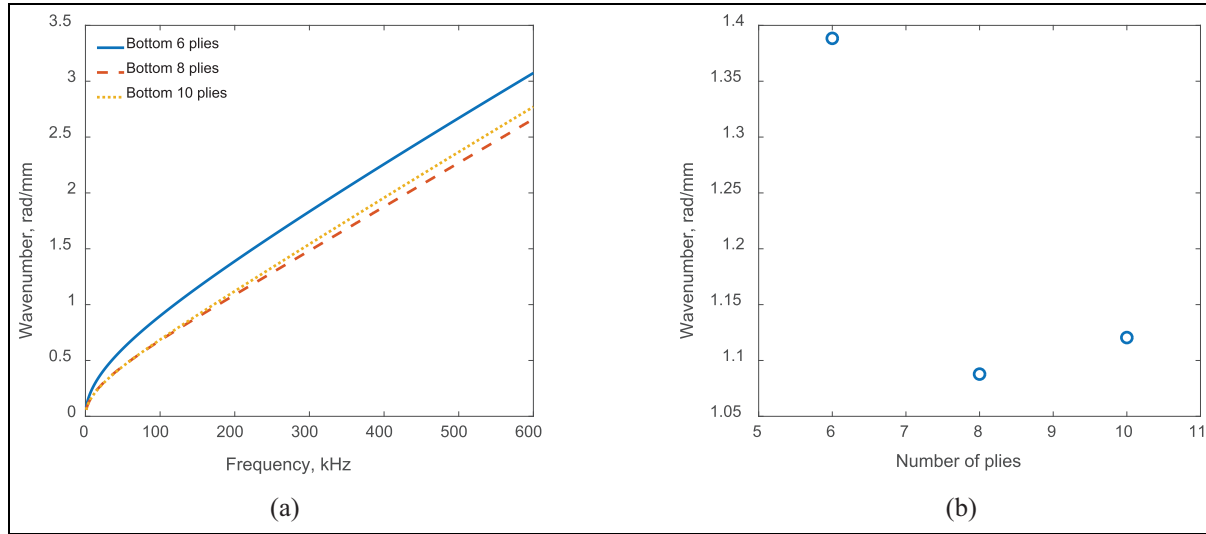Note: the number of plies is counted from the top of the full plate.
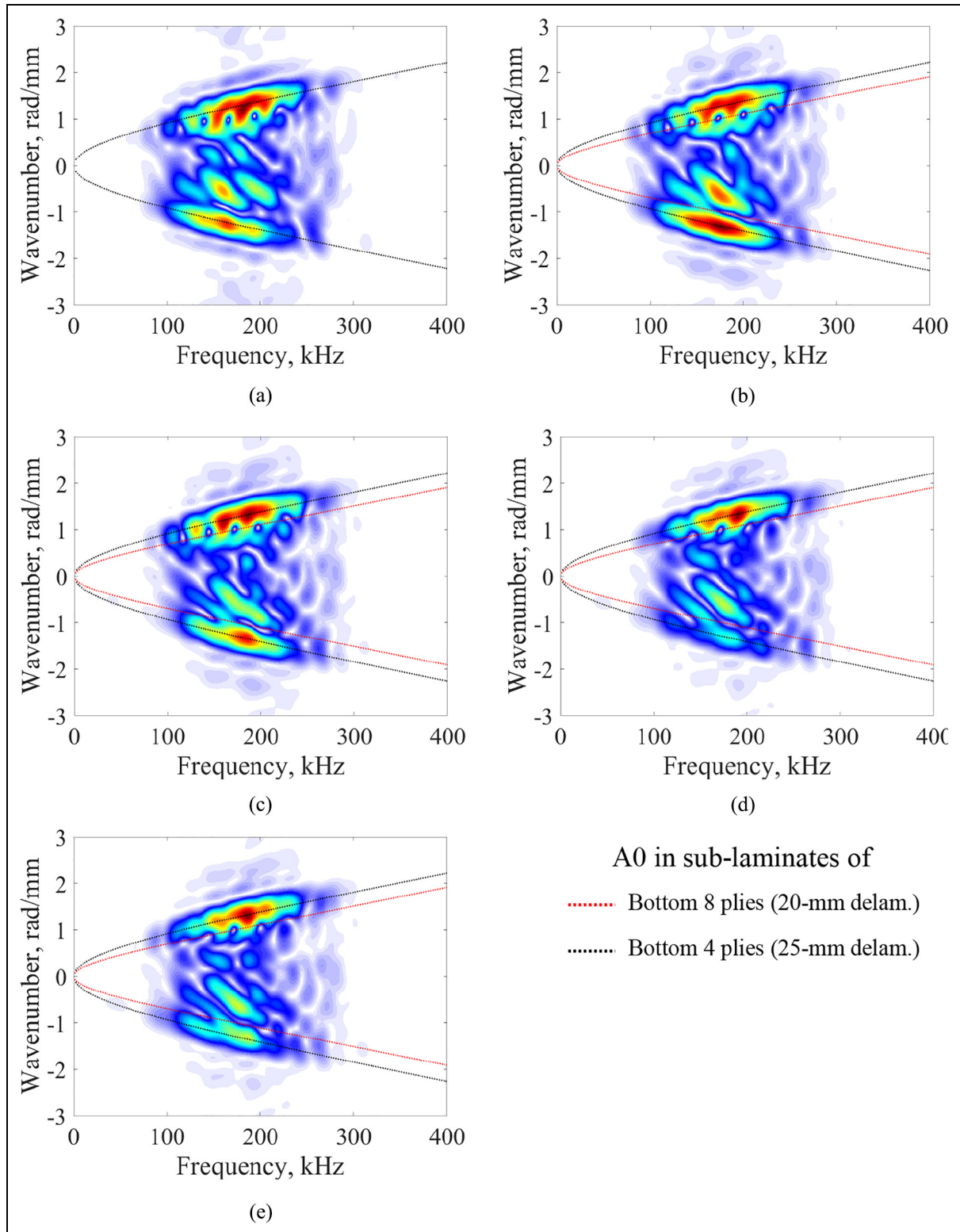
Figure 15. Frequency–wavenumber spectrums of the windowed wavefields on the bottom surface: (a) one delamination, (b) two delaminations, (c) three delaminations, (d) four delaminations, and (e) five delaminations.
Note: the number of plies is counted from the bottom of the full plate.

Figure 16. Delamination ply depth detection: (a) theoretical dispersion curve of A0 mode for different numbers of plies and (b) wavenumbers at 200 kHz versus the number of plies.

Note: the number of plies is counted from the bottom of the full plate.
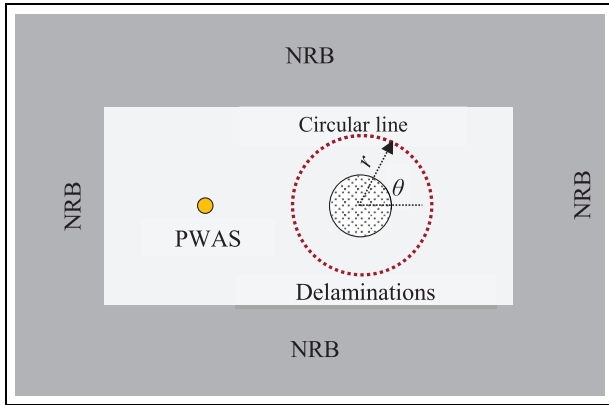
**Figure 17.** Schematic of scattering directivity pattern extraction from FEM simulations.

($\theta = 0°$). It can be found that the scattered wave amplitude increases significantly when an additional delamination appears. This is because the trapped wave energy increases with the delamination severity, which is consistent with the results reported in Leckey and Seebo.[42] In the case of a pitch–catch damage detection approach, it is likely that the delamination severity can be detected if the sensor is located in the forward direction of the incident wave.

Figure 19 shows the scattering directivity patterns of five different delamination cases. It can be found that the backward scattering amplitude is generally smaller than the forward scattering amplitude for all the

delamination cases. This is because weak scattered waves in the backward direction were captured due to the strong trapped waves in the delamination regions. However, a large amplitude loss was observed due to trapped waves in the forward direction, compared with the pristine signal. Therefore, a large forward scattering amplitude was observed for all the delamination cases. As a point of interest, the scattering pattern is not symmetric with respect to the 0° direction although the delamination is symmetric. This non-symmetric behavior of the scattering pattern is due to the non-symmetric layup for the sublaminates at the delamination regions and the non-symmetric distribution of incident wave amplitude. In addition, the forward scattering amplitude increases when the number of delaminations increases from one to three. Therefore, the delamination severity could be estimated by comparing the forward scattering amplitude for these three delamination cases.

However, for the cases of four and five delaminations, the forward scattering amplitudes slightly decreased, compared to the case of three delaminations. It should be noted that two sidelobes in the 30° and 330° directions were observed for the cases of four and five delaminations. In addition, the amplitude of the sidelobe increases when the number of delaminations increases from four to five. As shown in Figure 19, the scattering amplitudes around the directions perpendicular and opposite to the incident wave have relatively small amplitudes. Therefore, it is unlikely that the
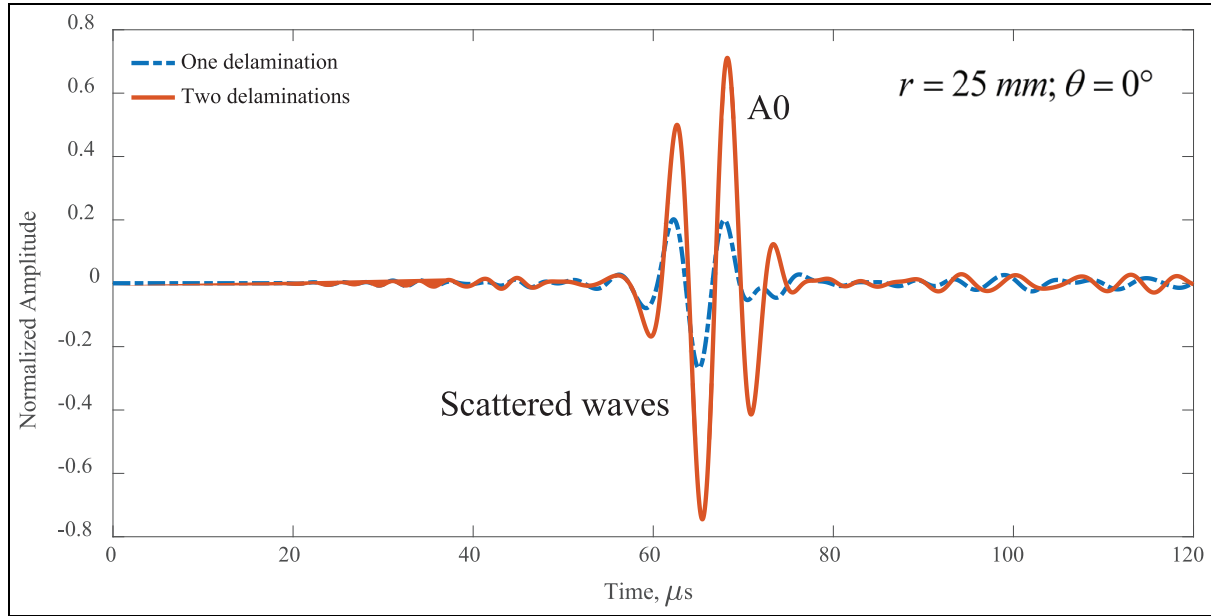
Figure 18. Waveform comparison of the scattered signals between one delamination and two delaminations in the 0° direction.

delamination can be detected if the sensor is located along these directions in a pitch–catch method.

Experimental validations

Experimental setup

Figure 20 shows the experimental setup of the hybrid SLDV-PWAS measurements. Two PWAS transducers (STEMINC SM412, 7 mm diameter and 0.5 mm thick) were mounted on the bottom surface to excite guided wave propagating in the 3-mm quasi-isotropic composite plate. The function generator (Tektronix AFG3052C) was used to generate a three-count Hanning window modulated tone burst with the center frequency of 200 kHz, which was amplified to 120 Vpp by the power amplifier (NF HSA4014) and applied to the PWAS transducers. Guided waves generated by the PWAS propagated in the composite plate, interacted with delaminations, and were measured by the SLDV (Polytec PSV-400-M2). The quantity measured by SLDV is the out-of-plane velocity. A thin reflective tape was attached to the plate surface to enhance the signal quality.

Experimental wavefield

From the FE simulation results, it can be found that strong wave interaction was observed when the measured surfaces are close to the delaminations. In this experiment, two SLDV area scans on the bottom surface were conducted for both one and two

delaminations to investigate the wave damage interaction. Figure 21(a) and (b) shows the transient spatial wavefields for one delamination and two delaminations, respectively. At 25 μs after the initial excitation, the lower amplitude S0 mode with a fast speed and a long wavelength and the higher amplitude A0 mode with a slow speed and a short wavelength can be clearly identified for both one and two delaminations, which agree well with the FEM predictions. In addition, weak trapped waves due to the S0 interactions with the delaminations were noted.

At 75 μs, after A0 waves interact with the multilayer delaminations, stronger trapped waves in the delamination regions were clearly observed, which are consistent with the simulation results in Figure 10. This is known as the wave trapping phenomenon.[29] Furthermore, the energy distributions of the wavefields were calculated to visualize the delaminations,[48] as shown in Figure 22. It was found that the approximate sizes of one and two delaminations can be estimated from the trapped waves in the delamination regions. However, it is not possible to separate the one and two delaminations by directly comparing the transient spatial wavefield. Therefore, wavenumber analysis was used to further analyze the experimental guided wavefield to compare with the results of FE simulations.

Wavenumber analysis

First, SLDV line scans were carried out across the delamination regions on the top surface for both one and
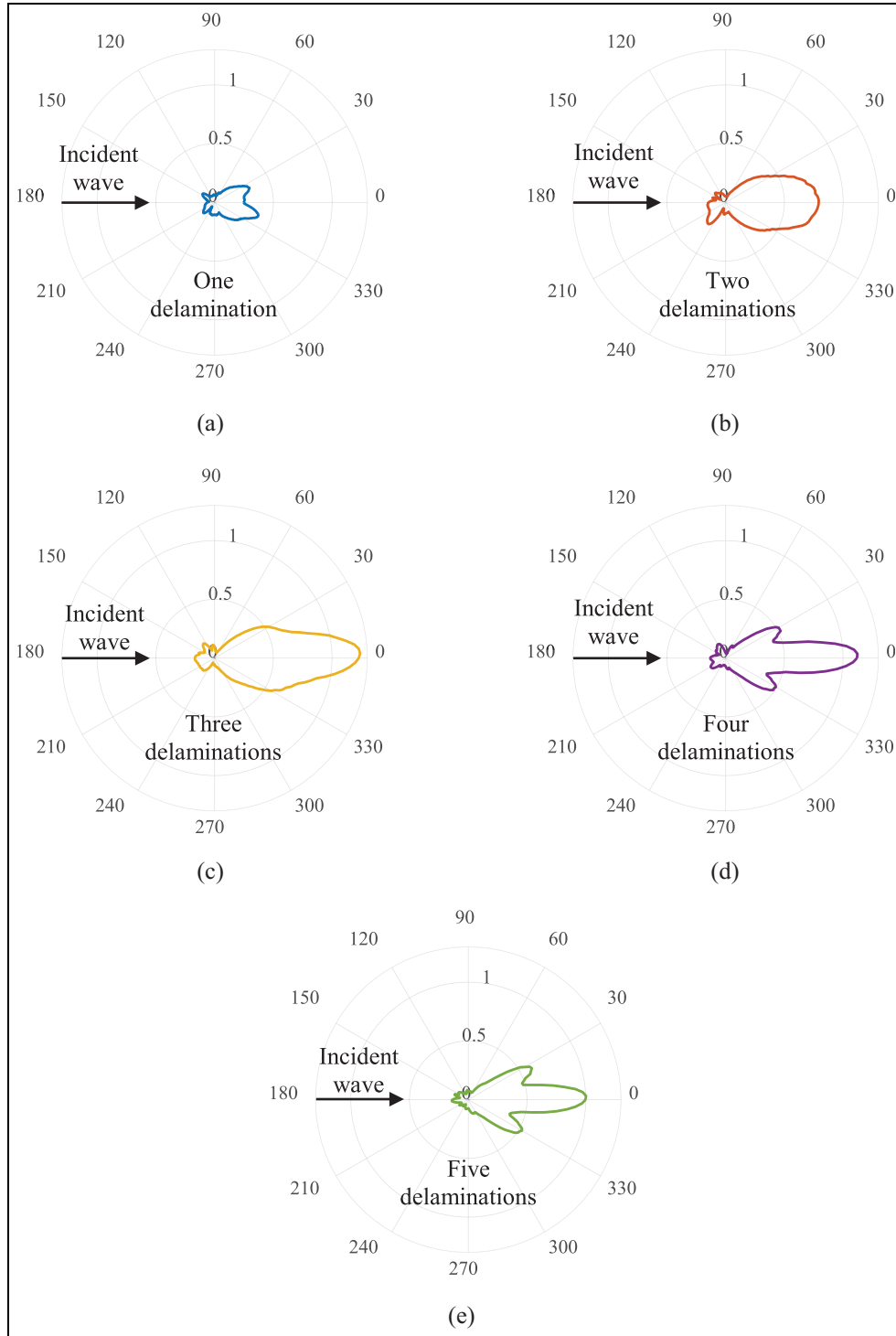
Figure 19. Comparison of the scattering directivity pattern at different delaminations: (a) one delamination, (b) two delaminations, (c) three delaminations, (d) four delaminations, and (e) five delaminations.

two delaminations. The time-space wavefields obtained on the top surface were given in Figure 23. Comparing to the out-of-plane FE wavefield in Figure 11(a) and (b), both wavefields show the existence of the higher amplitude A0 mode with a slow speed and the lower amplitude S0 mode with a fast speed. The experimental wavefield is much more dispersive than the FE simulations. Reflections were clearly observed at the delamination boundaries for both one and two delaminations.
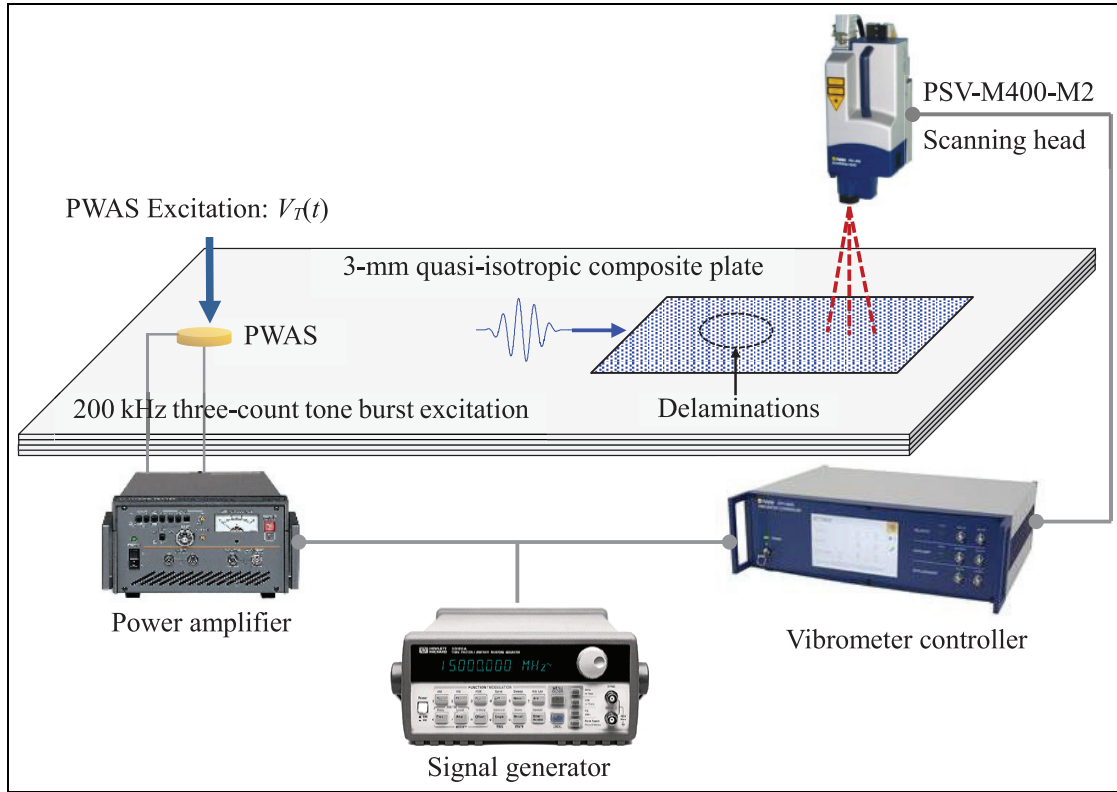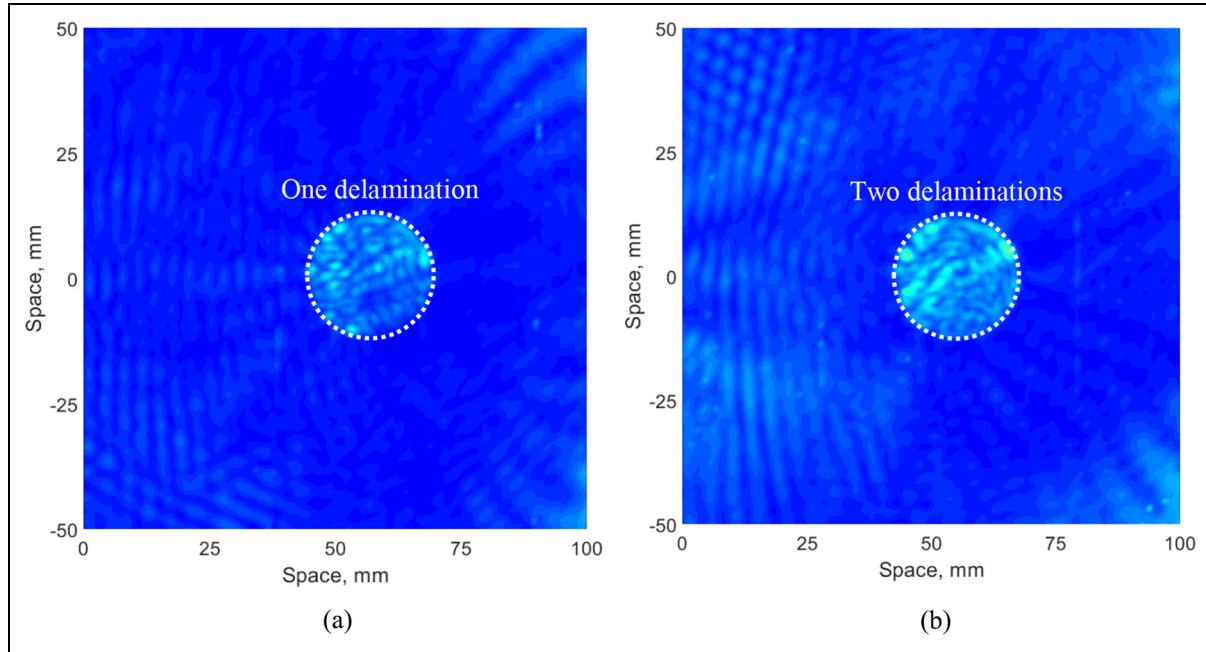
Figure 20. Experimental setup of the hybrid SLDV-PWAS measurements.

To obtain the experimental frequency–wavenumber spectrums, the measured time-space wavefields on the top surface were transformed into the frequency–wavenumber domain by 2D FFT. Figure 24 shows the comparison of experimental frequency–wavenumber spectrums on the top surface between one and two delaminations. Strong incident A0 mode (positive wavenumber) was observed in the frequency–wavenumber spectrums and agrees well with the theoretical dispersion curves (black lines in the spectrums). Comparing with the result of one delamination, a stronger negative wavenumber was observed for the case of two delaminations, which agrees well with the simulation in Figure 12. Experimental results confirmed that the more delaminations in the composite, the stronger reflections were observed. However, no obvious new wavenumbers can be observed in the wavenumber spectrum on the top surface, because it is far away from the delaminations.

The delamination ply depth can be identified when new wavenumbers are present in the wavenumber spectrum. To characterize the depth of the delaminations, SLDV line scans across the delamination region on the bottom surface were conducted. The time-space wavefield obtained on the bottom surface is shown in
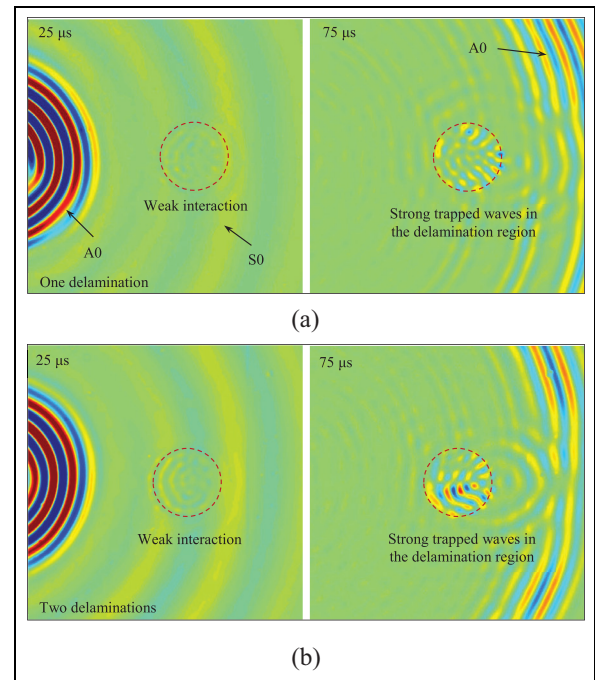
Figure 21. Comparison of the experimental transient spatial wavefield in the composite plate showing the out-of-plane velocity on the bottom surface: (a) one delamination and (b) two delaminations.

Figure 22. Comparison of the energy distribution of the wavefield in the composite plate: (a) one delamination and (b) two delaminations.
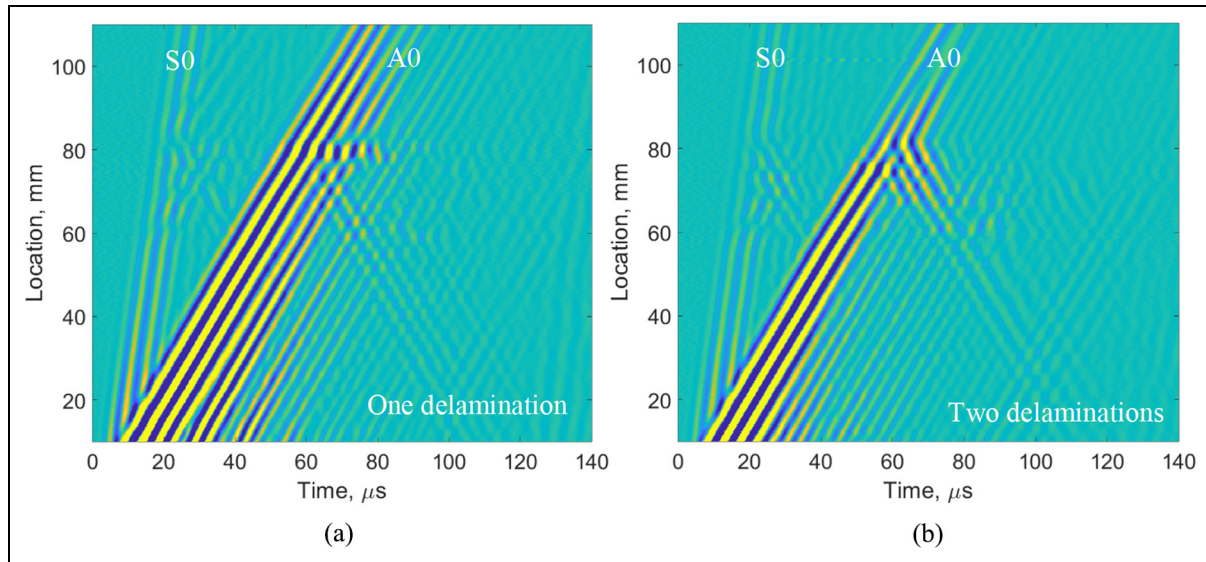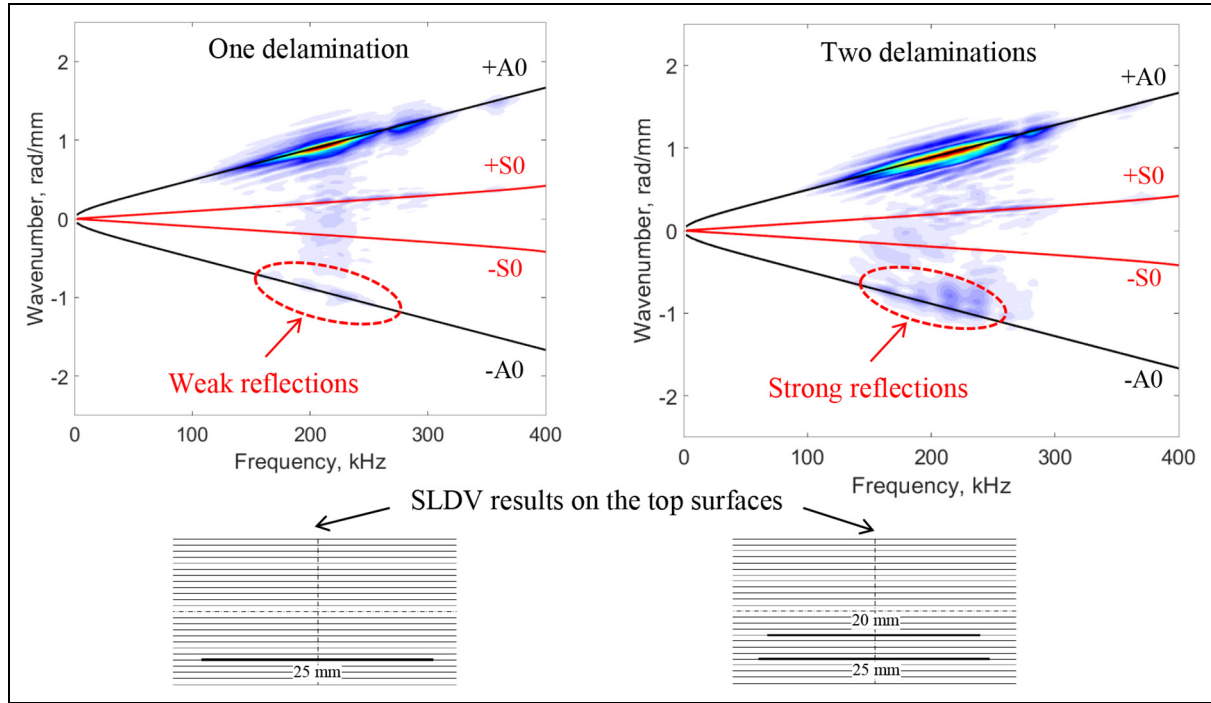

Figure 23. Time-space wavefield comparison of SLDV measurements on the top surface: (a) one delamination and (b) two delaminations.

Figure 25. The wavefield shows the higher amplitude A0 and the lower amplitude S0 mode as well. Similar to the simulation results in Figure 11(a) and (b), new strong trapped waves within the delamination regions can be clearly observed in both cases. To obtain the experimental frequency–wavenumber dispersion curves, the measured time-space wavefield was transformed into the frequency–wavenumber domain.

Figure 26 shows the comparison of experimental frequency–wavenumber spectrums between one and two delaminations. It can be found that new wavenumber components (both positive and negative) can be
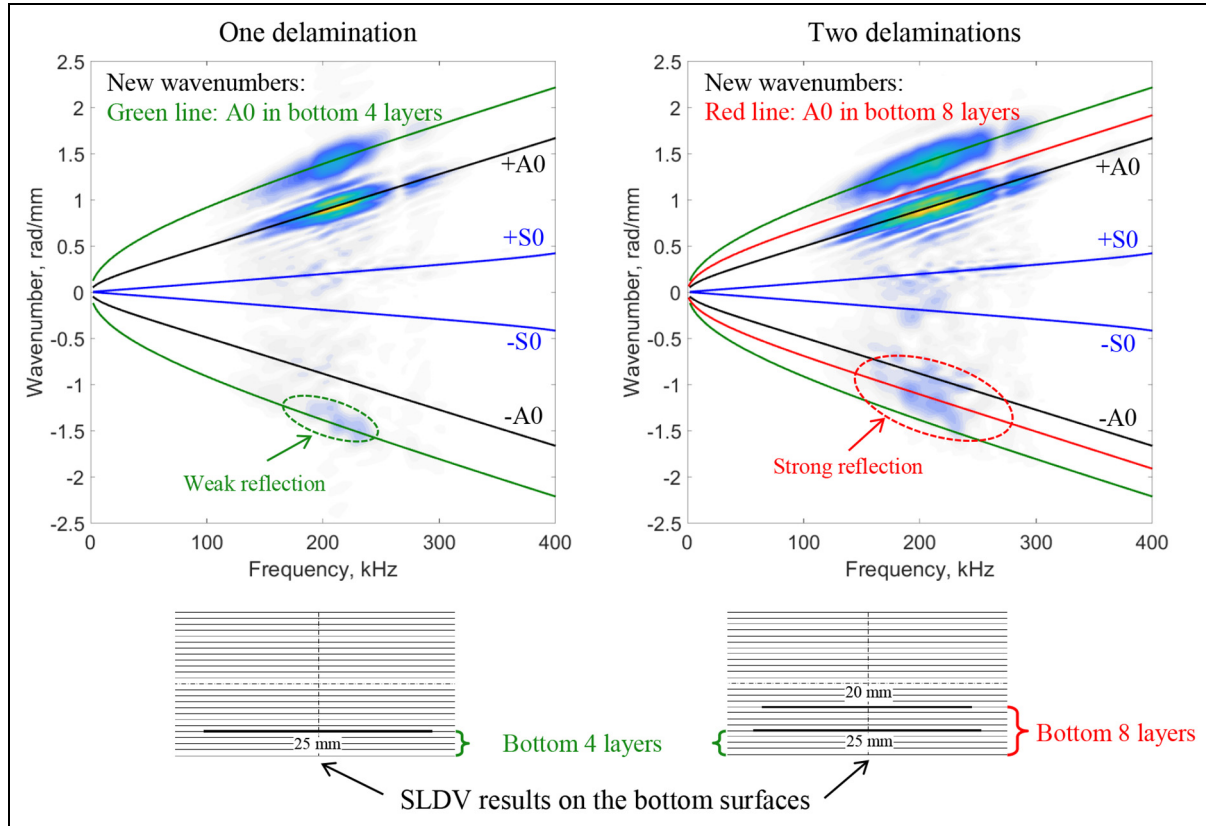
Figure 24. Frequency–wavenumber spectrum comparison of SLDV measurements on the top surface between one delamination and two delaminations.
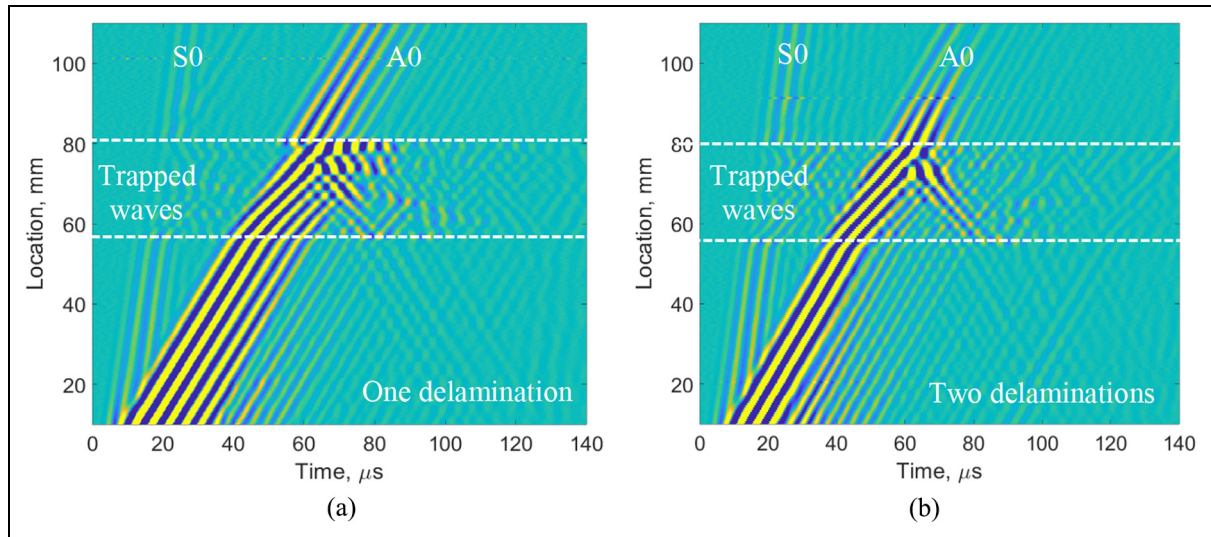
Figure 25. Time-space wavefield comparison of SLDV measurements on the bottom surface: (a) one delamination and (b) two delaminations.

observed, which agree well with the simulation results in Figure 13. The new wavenumber components are correlated to the wave propagation in the delamination regions. Comparing to the simulation, the experimental spectrum of one delamination also confirmed that the new wavenumber components are related to the A0 mode in the bottom four [−45/90/45/0] layers. Thus, the delamination was detected above the bottom fourth ply. From the experimental spectrum of two delaminations, besides the new wavenumber in bottom four layers, weak wavenumber components related to the A0 mode in the bottom eight layers were also observed

Figure 26. Frequency–wavenumber spectrum comparison of SLDV measurements on the bottom surface between one delamination and two delaminations.

for the case of two delaminations. Because there is an additional delamination between plies 16 and 17 (above bottom eighth ply).

Note that the new negative wavenumbers in the SLDV results are weaker than those in FE simulation (Figure 13). It is expected that this is due to the differences between Teflon inserts for the simulated delaminations in the experiment and the node detachment (zero volume delamination) in the simulation. The experimental results validate that strong new negative wavenumber due to the trapped waves in the delamination regions was observed when an additional delamination exists, which agrees well with the simulation results. It demonstrates that the more delaminations in the composite, the stronger wave energy was trapped. Therefore, the delamination severity can be characterized through the wavenumber analysis.

## Suggestion for practical implementations

It should be noted that the prior studies in guided wavefield analysis and the work presented in this article rely on the point-by-point SLDV scanning for recording wavefield data. However, point-by-point scanning

can be time-consuming which diminishes one of the main advantages of guided wave–based damage detection for practical applications, that is, rapid large-scale inspection. Thus, the work presented in this article can be viewed as providing deep physical insight into the guided wave interaction with multilayer delaminations, which can be used to validate and improve the performance of guided wave damage detection methods by selecting transducer locations and hence help to further advance the use of guided waves for delamination detection and characterization.

Both numerical and experimental results show that strong energy was trapped in the delamination region. In addition, stronger trapped waves and reflections were observed when the severity of delamination increased. In the case of a pitch–catch damage detection approach, it is likely that the delamination severity can be detected if the sensor is located in the forward direction of the incident wave.

For practical implementations, one suggestion is to use angle beam transducers to conduct a pitch–catch experiment for delamination detection, which has been demonstrated that it could be used for the rapid detection of different types of manufacturing flaws and
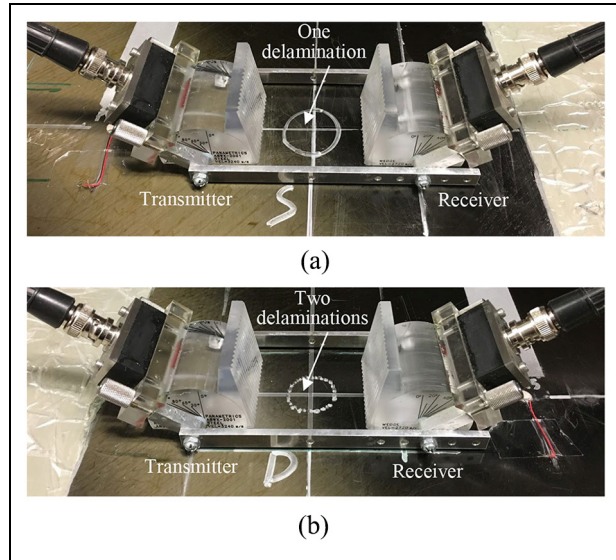
Figure 27. Experimental setup for delamination detection in the quasi-isotropic composite plate: (a) one delamination and (b) two delaminations.

operational damage in composite structures over large areas without doing point-by-point scanning.[49–52] For proof of concept, adjustable angle beam transducers were used as the transmitter and the receiver to generate pure-mode guided waves for the detection and characterization of multilayer delaminations.

In this study, pitch–catch experiments were conducted for both one and two delaminations, as shown in Figure 27. Two 500-kHz broadband angle beam transducers (Olympus A413S-SB) mounted on adjustable wedges (Olympus ABWX-2001) were used as the transmitter and the receiver. The adjustable angle beam transducer pair was used to generate a pure SH0 mode guided wave for the delamination detection in the 3-mm quasi-isotropic CFRP composite plate. The incident angle of the wedge was set to 48° for pure SH0 mode excitation at 500 kHz. The detailed experimental setup can be found in Mei et al.[51] A three-count Hanning-windowed tone burst at the central frequency of 500 kHz was used as the excitation signal. A spacing of 100 mm was ensured between transmitter and receiver using a rigid frame.

Signal comparison among the pristine and delaminations is shown in Figure 28. It can be found that strong and non-dispersive wave packets were clearly observed in the response signals and an amplitude drop can be clearly noted due to the presence of delaminations. Moreover, the amplitude further decreased when the delamination number increases from one to two, which is consistent with the numerical and experimental results in sections "Multiphysics FE simulation" and "Experimental validations," that is, the more

delaminations in the composite, the stronger wave energy was trapped.

Similarly, amplitude drop can be noted in the short-time Fourier transform (STFT) spectrograms as shown in Figure 28. It should be noted that the delamination spectrograms were normalized by the peak value of the pristine spectrogram. Therefore, the delaminations were successfully detected using the angle beam transducers. Moreover, one and two delaminations can be further distinguished based on the amplitude information of the received signals. The results demonstrate a potential technique for identifying and characterizing the presence of hidden multilayer delaminations in practical applications. It could be a very useful technique for the rapid large-area inspection.

Summary, conclusion, and future work

Summary

In this article, a numerical and experimental investigation on guided wave interaction with multilayer delaminations was conducted. First, two different delamination scenarios—one delamination and two delaminations—in a 3-mm quasi-isotropic $[-45/90/45/0]_{3s}$ CFRP composite plate were successfully verified and visualized through the ultrasonic C-scan. Then, a multiphysics 3D FE simulation of the composite plate with five different delamination scenarios was conducted to study guided wave interaction with multiple delaminations. Next, the simulation wavefield was validated by the SLDV measurements on the quasi-isotropic composite plate with multilayer delaminations. A good match was achieved between the simulation and the experiment. The wavefield data were further analyzed using wavenumber analysis to study the wave trapping phenomenon and to characterize the wave behaviors at the delamination regions. Finally, a pitch–catch experiment using angle beam transducers was conducted to detect the one and two delaminations. The results are a preliminary proof of concept for using trapped wave phenomena to evaluate the delamination severity.

Conclusion

Multiphysics FE simulations show strong trapped waves in the delamination regions when the measured surface is close to the delamination. The scattering directivity patterns of multilayer delaminations show that the backward scattering amplitude is smaller than the forward scattering amplitude. A larger forward scattering amplitude was observed when an additional delamination exists. In the case of a pitch–catch damage detection approach, it is likely that the
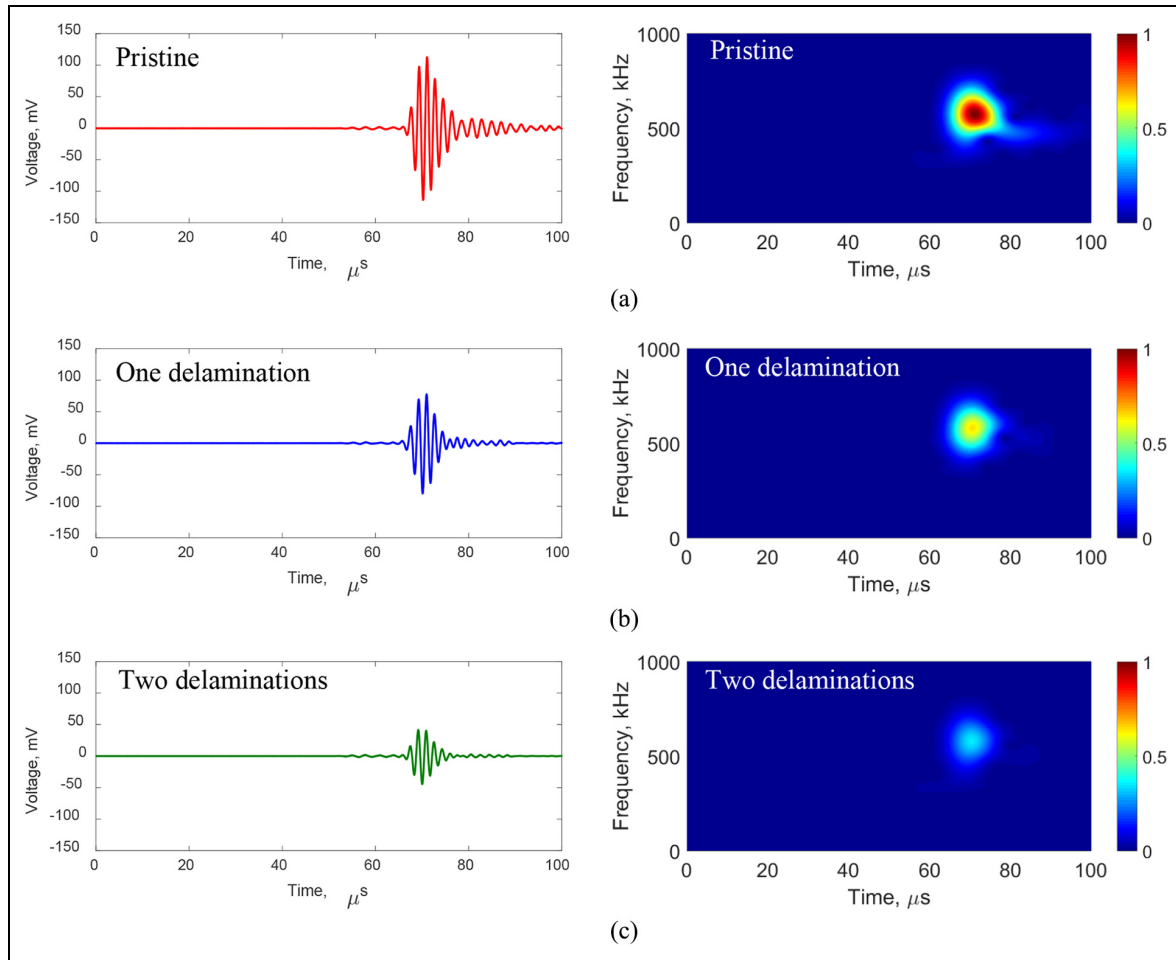
Figure 28. Comparison of waveforms and short-time Fourier transform (STFT) spectrograms: (a) pristine, (b) one delamination, and (c) two delaminations.

delamination can be detected if the sensor is located in the forward direction of the incident wave. The frequency–wavenumber spectrums indicate that the new wavenumbers come from the trapped waves in the delamination regions. The depth of the delamination near the measured surfaces was estimated by comparing and fitting the new wavenumber components to theoretical predictions calculated using the sublaminate thickness and layup of the delamination region. However, the estimation accuracy depends on the difference of the new wavenumbers in sublaminates. Both numerical and experimental results confirm that the new negative wavenumber due to the trapped waves in the delamination regions is potentially related to the delamination severity.

Future work

A higher excitation frequency will be used to characterize the multilayer delaminations. In addition, the current work would be extended to the simulation and experimental validation of guided wave interaction with low-velocity impact damage, which is a commonly observed damage in engineering applications. Impact damage is a combination of matrix cracking, fiber breakage, and interlaminar delamination. It is expected that guided waves would have a strong and complex interaction with the impact damage.

Declaration of conflicting interests

The author(s) declared no potential conflicts of interest with respect to the research, authorship, and/or publication of this article.

Funding

ORCID iD

Hanfei Mei https://orcid.org/0000-0002-8921-494X

References

1. Giurgiutiu V. *Structural health monitoring of aerospace composites*. London: Academic Press—Elsevier, 2016.
2. Flores M, Mollenhauer D, Runatunga V, et al. High-speed 3D digital image correlation of low-velocity impacts on composite plates. *Compos Part B: Eng* 2017; 131: 153–164.
3. Yuan S, Ren Y, Qiu L, et al. A multi-response-based wireless impact monitoring network for aircraft composite structures. *IEEE T Ind Electron* 2016; 63(12): 7712–7722.
4. Wilson CL and Chang FK. Monitoring fatigue-induced transverse matrix cracks in laminated composites using built-in acousto-ultrasonic techniques. *Struct Health Monit* 2016; 15(3): 335–350.
5. Su Z, Ye L and Lu Y. Guided Lamb waves for identification of damage in composite structures: a review. *J Sound Vib* 2006; 295(3–5): 753–780.
6. Shen Y and Cesnik CES. Hybrid local FEM/global LISA modeling of damped guided wave propagation in complex composite structures. *Smart Mater Struct* 2016; 25(9): 095021.
7. Mei H and Giurgiutiu V. Guided wave excitation and propagation in damped composite plates. *Struct Health Monit* 2019; 18(3): 690–714.
8. James R, Faisal Haider M, Giurgiutiu V, et al. A simulative and experimental approach toward eddy current nondestructive evaluation of manufacturing flaws and operational damage in CFRP composites. *J Nondestruct Eval* 2020; 3(1): 011002.
9. Cheng L and Tian GY. Comparison of nondestructive testing methods on detection of delaminations in composites. *J Sensors* 2012; 2012: 408437.
10. Zhang Z, Guo S, Li Q, et al. Ultrasonic detection and characterization of delamination and rich resin in thick composites with waviness. *Compos Sci Technol* 2020; 189: 108016.
11. Wallentine SM and Uchic MD. A study on ground truth data for impact damaged polymer matrix composites. *AIP Conf Proc* 2018; 1949(1): 120002.
12. Mei H, Faisal Haider M, Joseph R, et al. Recent advances in piezoelectric wafer active sensors for structural health monitoring applications. *Sensors* 2019; 19(2): 383.
13. Gresil M, Yu L, Giurgiutiu V, et al. Predictive modeling of electromechanical impedance spectroscopy for composite materials. *Struct Health Monit* 2012; 11(6): 671–683.
14. Nikbakht M, Yousefi J, Hosseini-Toudeshky H, et al. Delamination evaluation of composite laminates with different interface fiber orientations using acoustic emission features and micro visualization. *Compos Part B: Eng* 2017; 113: 185–196.
15. Mei H, Migot A, Faisal Haider M, et al. Vibration-based in-situ detection and quantification of delamination in composite plates. *Sensors* 2019; 19(7): 1734.
16. De Luca A, Caputo F, Sharif Khodaei Z, et al. Damage characterization of composite plates under low velocity impact using ultrasonic guided waves. *Compos Part B: Eng* 2018; 138: 168–180.
17. Dafydd I and Sharif Khodaei Z. Analysis of barely visible impact damage severity with ultrasonic guided Lamb waves. *Struct Health Monit*. Epub ahead of print 30 September 2019. DOI: 10.1177/1475921719878850.
18. Chang HY and Yuan FG. Damage imaging in a stiffened curved composite sandwich panel with wavenumber index via Riesz transform. *Struct Health Monit* 2020; 19: 902–916.
19. Staszewski WJ, Mahzan S and Traynor R. Health monitoring of aerospace composite structures—active and passive approach. *Compos Sci Technol* 2009; 69(11–12): 1678–1685.
20. Tian Z, Yu L and Leckey CAC. Delamination detection and quantification on laminated composite structures with Lamb waves and wavenumber analysis. *J Intel Mat Syst Str* 2015; 26(13): 1723–1738.
21. Rogge MD and Leckey CAC. Characterization of impact damage in composite laminates using guided wavefield imaging and local wavenumber domain analysis. *Ultrasonics* 2013; 53(7): 1217–1226.
22. Juarez PD and Leckey CAC. Multi-frequency local wavenumber analysis and ply correlation of delamination damage. *Ultrasonics* 2015; 62: 56–65.
23. Mesnil O, Leckey CAC and Ruzzene M. Instantaneous and local wavenumber estimations for damage quantification in composites. *Struct Health Monit* 2015; 14(3): 193–204.
24. Mesnil O, Yan H, Ruzzene M, et al. Fast wavenumber measurement for accurate and automatic location and quantification of defect in composite. *Struct Health Monit* 2016; 15(2): 223–234.
25. Zhao G, Wang B, Hao W, et al. Localization and characterization of delamination in laminates using the local wavenumber method. *Compos Struct* 2020; 238: 111972.
26. Ruzzene M. Frequency–wavenumber domain filtering for improved damage visualization. *Smart Mater Struct* 2007; 16(6): 2116.
27. Michaels TE, Michaels JE and Ruzzene M. Frequency–wavenumber domain analysis of guided wavefields. *Ultrasonics* 2011; 51(4): 452–466.
28. Park B, An YK and Sohn H. Visualization of hidden delamination and debonding in composites through non-contact laser ultrasonic scanning. *Compos Sci Technol* 2014; 100: 10–18.
29. Sohn H, Dutta D, Yang JY, et al. Delamination detection in composites through guided wave field image processing. *Compos Sci Technol* 2011; 71(9): 1250–1256.
30. He J and Yuan FG. A quantitative damage imaging technique based on enhanced CCRTM for composite plates using 2D scan. *Smart Mater Struct* 2016; 25(10): 105022.
31. Girolamo D, Chang HY and Yuan FG. Impact damage visualization in a honeycomb composite panel through laser inspection using zero-lag cross-correlation imaging condition. *Ultrasonics* 2018; 87: 152–165.

32. Eremin A, Glushkov E, Glushkova N, et al. Guided wave time-reversal imaging of macroscopic localized inhomogeneities in anisotropic composites. *Struct Health Monit* 2019; 18(5–6): 1803–1819.

33. Tian Z, Yu L, Leckey CAC, et al. Guided wave imaging for detection and evaluation of impact-induced delamination in composites. *Smart Mater Struct* 2015; 24(10): 105019.

34. Kudela P, Radzienski M and Ostachowicz W. Impact induced damage assessment by means of Lamb wave image processing. *Mech Syst Signal Pr* 2018; 102: 23–36.

35. Guo N and Cawley P. The interaction of Lamb waves with delaminations in composite laminates. *J Acoust Soc Am* 1993; 94(4): 2240–2246.

36. Ramadas C, Balasubramaniam K, Joshi M, et al. Interaction of the primary anti-symmetric Lamb mode (A_o) with symmetric delaminations: numerical and experimental studies. *Smart Mater Struct* 2009; 18(8): 085011.

37. Ramadas C, Balasubramaniam K, Joshi M, et al. Interaction of guided Lamb waves with an asymmetrically located delamination in a laminated composite plate. *Smart Mater Struct* 2010; 19(6): 065009.

38. Munian RK, Mahapatra DR and Gopalakrishnan S. Lamb wave interaction with composite delamination. *Compos Struct* 2018; 206: 484–498.

39. Leckey CAC, Wheeler KR, Hafiychuk VN, et al. Simulation of guided-wave ultrasound propagation in composite laminates: benchmark comparisons of numerical codes and experiment. *Ultrasonics* 2018; 84: 187–200.

40. Ng CT and Veidt M. Scattering of the fundamental antisymmetric Lamb wave at delaminations in composite laminates. *J Acoust Soc Am* 2011; 129(3): 1288–1296.

41. Murat BIS, Khalili P and Fromme P. Scattering of guided waves at delaminations in composite plates. *J Acoust Soc Am* 2016; 139(6): 3044–3052.

42. Leckey CAC and Seebo JP. Guided wave energy trapping to detect hidden multilayer delamination damage. *AIP Conf Proc* 2015; 1650(1): 1162–1169.

43. Leckey CAC, Rogge MD and Parker FR. Guided waves in anisotropic and quasi-isotropic aerospace composites: three-dimensional simulation and experiment. *Ultrasonics* 2014; 54(1): 385–394.

44. Zhang B, Sun XC, Eaton MJ, et al. An integrated numerical model for investigating guided waves in impact-damaged composite laminates. *Compos Struct* 2017; 176: 945–960.

45. Barazanchy D, Roth W and Giurgiutiu V. A nondestructive material characterization framework for retrieving a stiffness matrix using bulk waves. *Compos Struct* 2018; 185: 27–37.

46. Tian Z and Yu L. Lamb wave frequency–wavenumber analysis and decomposition. *J Intel Mat Syst Str* 2014; 25(9): 1107–1123.

47. Shen Y and Giurgiutiu V. Effective non-reflective boundary for Lamb waves: theory, finite element implementation, and applications. *Wave Motion* 2015; 58: 22–41.

48. Xiao W and Yu L. Nondestructive evaluation of nuclear spent fuel dry cask structures using non-contact ACT-SLDV Lamb wave method. In: *Proceedings of the SPIE smart structures and NDE for industry 4.0, smart cities, and energy systems*, 27 April–8 May 2020, vol. 11382, p. 113820D. Bellingham, WA: International Society for Optics and Photonics.

49. Toyama N and Takatsubo J. Lamb wave method for quick inspection of impact-induced delamination in composite laminates. *Compos Sci Technol* 2004; 64(9): 1293–1300.

50. Mei H, James R, Faisal Haider M, et al. Multimode guided wave detection for various composite damage types. *Appl Sci* 2020; 10(2): 484.

51. Mei H, Faisal Haider M, James R, et al. Pure S0 and SH0 detections of various damage types in aerospace composites. *Compos Part B: Eng* 2020; 189: 107906.

52. Wang K, Liu M, Cao W, et al. Detection and sizing of disbond in multilayer bonded structure using modally selective guided wave. *Struct Health Monit*. Epub ahead of print 2 August 2019. DOI: 10.1177/1475921719866274.